Astrocyte to microglia cross-talk in acute and chronic neuroinflammation is shaped by SFRP1

Javier Rueda-Carrasco[1,2], María Inés Mateo[1,2], Aldo Borroto[1], María Jesús Martin-Bermejo[1,2], Markus P. Kummer[3,4], Stephanie Schwartz[3,4]; José P. López-Atalaya[5]; Balbino Alarcon[1], Michael T. Heneka[3,4], Pilar Esteve[1,2] and Paola Bovolenta[1,2*]

[1]Centro de Biología Molecular Severo Ochoa, CSIC-UAM, c/ Nicolás Cabrera, 1, Campus de la Universidad Autónoma de Madrid, Madrid 28049, Spain; [2]CIBER de Enfermedades Raras (CIBERER) Madrid 28049, Spain; [3]Universitätsklinikum Bonn, Neurology; [4]German Center for Neurodegenerative Diseases (DZNE) 53127 Bonn, Germany. [5]Instituto de Neurociencias, CSIC-UMH, Sant Joan d'Alacant, Spain

Running title: SFRP1 enhances microglial activation

Key words: Neuroinflammation; HIF pathway; LPS; EAE; reactive astrocytes; multiple sclerosis; Alzheimer's disease

* corresponding author at pbovolenta@cbm.csic.es

Total character count: about 48,000

Abstract

Neuroinflammation is a common feature of many neurodegenerative diseases, which often enhances neuronal loss and fosters a dysfunctional neuron-microglia-astrocyte crosstalk that, in turn, maintains microglial cells into a perniciously reactive state. The molecular components that mediates this critical communication are however non-fully explored. Here, we have asked whether Secreted-Frizzled-Related-Protein 1 (SFRP1), a multifunctional regulator of cell to cell communication, is part of the cellular crosstalk underlying neuroinflammation. We show that in mouse models of acute and chronic neuroinflammation, astrocyte-derived SFRP1 is sufficient to promote microglial activation and to enhance their response to damage, sustaining a chronic inflammatory state. SFRP1 allows the upregulation of components of Hypoxia Induced Factors-dependent inflammatory pathway and, to a much lower extent, of those downstream of the Nuclear Factor-kappaB. We thus propose that SFRP1 acts as a critical astrocyte to microglia amplifier of neuroinflammation, representing a potential valuable therapeutic target for counteracting the harmful effect of chronic inflammation present in several neurodegenerative diseases.

Introduction

Degeneration of neurons occurs in a variety of rare and common pathological conditions of the Central Nervous System (CNS) including, for example, Alzheimer's disease (AD). CNS function is supported by a robust neurons-glia crosstalk (1, 2), so that neuronal damage is almost invariably associated with the activation of two types of glial cells: microglia and astrocytes. The prompt response of these glial cells to insults brings about an inflammatory reaction that favours tissue healing and helps restoring CNS homeostasis (3, 4). However, excessive glial activation, as often occurs in neurodegeneration, is itself a cause of neuronal loss, which, in turn, establishes a state of pernicious chronic neuroinflammation (4-7). Consistent with an important cellular crosstalk, glial cell dysfunction, either as a consequence of hyper or hypo functionality, can also be the cause of neuronal cell death, rather than its consequence, strongly contributing to the progression of neurodegenerative diseases (3, 4, 8, 9). Although this is nowadays a widely accepted idea, there is still only partial information on the molecular components that sustain a dys- or hyper-functional state of glial cells as well as an abnormal crosstalk among glia and neurons. Here we have investigated whether SFRP1 may represent one of such components.

SFRP1 is a small, secreted and dispersible protein with a dual function: modulation of Wnt signalling (10) and inhibition of ADAM10 activity (11). The latter function is particularly relevant in the context of neurodegeneration because ADAM10, a member of the A Disintegrin and Metalloprotease family of cell surface proteins (12), acts as an α–secretase (or sheddase; (13) for a large number of substrates expressed in both neurons and glial cells. In microglial cells, ADAM10-mediated shedding of TREM2 (Triggering Receptor Expressed on Myeloid) is a relevant mechanism for controlling their activation (14). In neurons, ADAM10 activity releases the ectodomain of CD200 and CX_3CL1 (15, 16), two components of the mechanism by which neurons maintain microglial cells in a surveying state (1). Consistent with these roles and the additional regulation of proteins involved in synapse formation (12, 17), genetic inactivation of *Adam10* in mice causes neuroinflammation and loss of synaptic plasticity (18). Interest in ADAM10 is further increased by genetic studies supporting a link between impaired ADAM10 activity and AD (19, 20). Thus, and based on its non-amyloidogenic processing of the Amyloid Precursor Protein (APP) (21), ADAM10 may have a protective role against AD (22). Consistent with this possibility, we have recently shown that elevated levels of SFRP1, its endogenous negative modulator, contribute to AD pathogenesis (23). SFRP1 upregulation correlates with poor ADAM10-mediated processing of APP and of the synaptic protein N-

Cadherin (23), whereas neutralization of its activity prevents the appearance of AD pathological traits, including glial cell activation (23). Whether SFRP1 is directly involved in the modulation of neuroinflammation remained however unexplored.

By addressing this issue, here we show that Sfrp1 is a novel mediator of the astrocyte to microglia crosstalk that underlies mammalian CNS inflammation. In mice, astrocyte-derived SFRP1 is sufficient to activate microglial cells and to amplify their response to distinct acute and chronic neuroinflammatory challenges, sustaining their chronic activation. From a molecular point of view, SFRP1 allows for the full expression of down-stream targets of the transcription factors hypoxia induced factors (HIF) and, to a lesser extent, nuclear factor-kappa B (NF-κB), which are mediators of neuroinflammatory responses (24, 25). Thus, neutralizing SFRP1 function may represent a strategy to counteract pernicious chronic neuroinflammation that contributes to many neurodegenerative conditions.

Results

Acute brain neuroinflammation elevates astrocyte-specific levels of SFRP1 expression

Sfrp1 is abundantly expressed in the mammalian radial glial progenitors of the developing CNS (26-28) and it is then largely downregulated in the adult brain with the exception of restricted neurogenic areas (26, 29, 30). Up-regulation of SFRP1 expression has been reported in a number of inflammatory conditions (10) as well as in the aged brain (31), which is characterized by a low-grade chronic inflammation (32). Elevated SFRP1 levels have been also observed in neurodegenerative diseases (23, 31, 33), with high levels of mRNA localized to glial cells (23, 30), pointing to a possible link between SFRP1 and neuroinflammation.

To evaluate this possibility, we induced acute brain inflammation by injecting bacterial lipopolysaccharides (LPS; (34) or control saline into the somatosensory cortex of 3 months-old *Sfrp1*$^{+/\beta gal}$;*CX*$_3$*CR1*$^{+/GFP}$ mice (n=4), which allow the simultaneous identification of microglial (GFP; (35) and *Sfrp1* producing cells (marked by nuclear βgal; (36). Immunofluorescence analysis of the brains three days after injection, when inflammation is at its peak (37), revealed a broader βgal immunoreactivity (as a reporter of *Sfrp1* expression) in LPS vs saline treated animals (Fig. 1a), largely localised in GFAP$^+$ astrocytes but not in Iba1$^+$ microglial cells (Fig. 1a). Immunodetection of SFRP1 with specific antibodies (23) confirmed an increased SFRP1 production after LPS but not saline injections (Fig. 1b). Consistent with the secreted and dispersible nature of SFRP1 (27, 38), immuno-signal was widely distributed in the brain parenchyma with a more abundant localisation around GFAP$^+$ astrocytic processes and GFP$^+$ microglial cells (arrows in Fig. 1b). The use of a highly specific ELISA (23) further confirmed a significant increase of SFRP1 levels in extracts of small cortical tissue samples from LPS vs saline treated animals (n=5; Fig. 1c).

Together these data show that astrocytes produce and secrete increased level of SFRP1 in response to a bacterial lipopolysaccharide.

In vivo Sfrp1 gene addition is sufficient to trigger and sustain glial cell activation

We next reasoned that if SFRP1 is indeed associated with neuroinflammation, its forced expression should be sufficient to activate glial cells. To test this possibility, we infused lentiviral vectors (LV) containing *Sfrp1*-IRES-*Gfp* or control IRES-*Gfp* into the lateral ventricle of 10 weeks-old wt mice (n=8; Fig. 2). As expected by the injection site, GFP$^+$ (used to determine infection efficiency) LV-transduced cells were largely found along the wall of the lateral ventricle, in the choroid plexus and, to a less extent, along the rostral migratory stream

(Fig. 2a). Immunohistochemistry of cortical sections 1 month after injection showed a significantly higher presence GFAP+ reactive astrocytes and Iba1+ microglial cells as compared to LV-IRES-*Gfp* control animals (Fig. 2b, c; quantifications performed in 3 of the injected animals). Iba1 immunoreactivity was accumulated around the injection site (Fig. 2b, c) and many cells had a round amoeboid morphology with a significantly higher expression of the CD45 antigen (Fig. 2b-d), two characteristics of reactive microglia (39). A wider distribution of hyper-phosphorylated Tau, which often appears as a response of the brain to inflammation and degeneration (40), was also detected in LV-*Sfrp1*-IRES-*Gfp* transduced vs control sections (Fig. 2b, c).

The glial response to SFRP1 was not transient. Indeed, analysis of a different set of LV-transduced animals (n=4) 5 months after LV delivery showed a persistent microglial activation in SFRP1- vs GFP-treated animals, with a larger number of CD45+ cells than those observed at 1-month post-injection (Fig. 2d). Furthermore, several CD45hi-round-shaped cells were detected in the brain parenchyma, especially in the proximity of the transduced cells, likely representing infiltrated macrophages or lymphocytes (39); arrowheads in Fig. 2d).

Together these results indicate that upregulation of SFRP1 levels is sufficient to trigger and sustain microglial cell activation.

Sfrp1 is required for amplifying CNS inflammatory response

Given that SFRP1 was sufficient to induce glial cell activation, we next asked whether it was also a necessary component of the CNS inflammatory response. To this end, we took advantage of *Sfrp1*-/- mice. These mice have a slightly shorter and thicker cortex that however does not affect their life span, reproduction rate or cognitive and motor behaviour (23, 26). Furthermore, their content of astrocytes and microglial cells was undistinguishable from that of wt mice (Fig. 3). We thus compared the effect of intra-cortical LPS infusion into the brains of 3-months-old wt and *Sfrp1*-/- mice (Fig. 3). In wt brains, LPS but not saline treatment caused the appearance of GFAP+ reactive astrocytes (Fig. 3a) and CD45+ reactive microglia (Fig. 3b) even at a distance from the injection site. In contrast, *Sfrp1*-/- littermates presented fewer and less immuno-positive astrocytes and a significant reduction of CD45+ reactive microglia (Fig. 3a, b), suggesting that SFRP1 is relevant for astrocytic and microglial activation. Quantitative comparison of GFAP and CD45 immunoreactivity among different genotypes and treatments confirmed no significant differences between the two saline-treated genotypes (Fig. 3c,d). However, the response of *Sfrp1*-/- mice to LPS infusion was significantly reduced compared to wt mice, although significantly different from that observed in saline injection (Fig. 3c,d).

To evaluate the specificity of this response to LPS, we induced Experimental Autoimmune Encephalomyelitis (EAE) in wt and *Sfrp1*$_{-/-}$ mice. This is a widely used experimental model for the human inflammatory demyelinating disease, Multiple Sclerosis (MS). In EAE, CNS inflammation and gliosis occur as a consequence of a strong autoimmune response against the peripheral exposure to myelin components (41), thus representing a neuroinflammatory paradigm quite different from the direct intra-cerebral infusion of LPS. Female littermates of the two genotypes were immunised following a standard protocol and animals were scored for the development/remission of their clinical symptoms over the course of a month (42). Animals were classified with a standard 0 to 5 rank based on their paralysis degree, with 0 corresponding to absence of symptoms and 5 to a moribund condition (42). In wt mice (n=19), tail limping -the first symptom of the disease- became apparent around 8 days after immunization with a subsequent rapid progression, so that, by 16 days, most of the wt animals presented hind limb paralysis followed by a slow recovery (Fig. 4a). Notably, 47% of the immunized wt mice developed extreme and protracted symptoms. The response of *Sfrp1*$_{-/-}$ mice (n=19) to immunization was instead slower and milder: only 16% of them developed extreme symptoms and their recovery was significantly faster (Fig. 4a). Immunostaining of spinal cord sections from animals (n=4) sacrificed 16 days after immunization, demonstrated a significant reduction of pathological signs in *Sfrp1*$_{-/-}$ vs. wt mice, including infiltration of CD4$_{+}$ lymphocytes, presence of Iba1$_{+}$ macrophages/activated microglial cells and GFAP+ reactive astrocytes, pial surface disruption and loss of MBP$_{+}$ myelin (Fig. 4b, c).

All in all, these data indicate that SFRP1 is commonly required for a robust neuroinflammatory response, likely mediating astrocyte to microglial crosstalk.

Astrocyte-derived Sfrp1 is required for a robust response of microglial cells to damage

The latter possibility found support in SFRP1 localization around microglial cells (Fig. 1b) and in the remarkably poor microglial activation (Fig. 3 and 4) and myeloid cell recruitment (Fig. 4b) observed in the absence of *Sfrp1*. To further explore this possibility we used flow cytometry analysis to determine the proportion of the different CD11b$_{+}$ myeloid populations (43) in the cortex of *CX$_3$CR1*$_{+/GFP}$ and *CX$_3$CR1*$_{+/GFP}$;*Sfrp1*$_{-/-}$ mice 3 days after intra-cerebro-ventricular LPS or saline administration (Fig. 5a). In the absence of *Sfrp1*, there was a significant decrease of the LPS-induced infiltration of CD11b$_{+}$;CD45$_{+}$;GFP$_{-}$ monocytes and of the proportion of microglial cells that passed from a CD11b$_{+}$;CD45$_{lo}$;GFP$_{+}$ surveying to a CD11b$_{+}$;CD45$_{+}$;GFP$_{+}$ activated state (Fig. 5a, b). Furthermore, upon infusion of pHrodo *E.coli* bioparticles (44) into the third ventricle, *CX$_3$CR1*$_{+/GFP}$;*Sfrp1*$_{-/-}$ mice showed less cumulative phagocytized fluorescent

signal than that of *CX3CR1+/GFP* mice at both 40 and 65 hr post infusion (Fig. 5c). Notably, at 40 hr the percentage of phagocyting cells in *CX3CR1+/GFP;Sfrp1-/-* mice was significantly higher than in controls (Fig. 5c). This increased proportion however underwent a drastic reduction at 65 hr (Fig. 5c).

Collectively, these data support the contention that SFRP1, likely derived from astrocytes (Fig. 1), modulates microglial activation in response to an inflammatory challenge and favours their efficient function. To assess that indeed there is an astrocyte-to-microglial flux of information, we next established microglial or astrocyte/microglia mixed cultures from wt and *Sfrp1-/-* neonatal mice and used a multiplex ELISA to determine their cytokines' release (IFNγ, TNFα, IL1-β, IL4, IL6 and IL10) in the culture medium, as a measure of their LPS-induced activation (39). After 24 hr, LPS but not saline treatment enhanced the accumulation of all tested cytokines in the culture media of purified microglial cultures with no significant differences between genotypes (Fig. 6). In astrocytes/microglia cultures derived from *Sfrp1-/-* LPS-induced cytokines' release was instead significantly reduced, as compared to that detected in similar wt-derived cultures (Fig. 6), strongly supporting that astrocyte-derived SFRP1 enhances microglial activation.

Sfrp1 allows for the full expression of down-stream targets of HIF transcription factors

We next reasoned that if SFRP1 enhances microglial activation, its absence should modify their transcriptomic profiling towards a less activated or surveying state. To test this possibility, we used fluorescence-associated cell sorting to purify GFP+ microglial cells from the brain of *CX3CR1+/GFP* and *CX3CR1+/GFP;Sfrp1-/-* mice (n=4). Cells were purified three days after the injection of LPS or saline and used to obtain the corresponding transcriptomic profiles. We initially compared the gene-expression signature of *CX3CR1+/GFP* and *CX3CR1+/GFP;Sfrp1-/-* derived microglial cells in response to LPS (Fig. 7). Principal-component analysis demonstrated LPS as the main source of variation (72% variance), whereas only 6% of the total variations could be attributed to the genotype after secondary-component analysis (Fig. 7a, Table S1-4), well in line with the observation that SFRP1 is poorly expressed in the adult brain under homeostatic conditions (Fig. 1; (23). The relatively central position of LPS-treated *Sfrp1-/-* microglia supported their milder inflammatory response (Fig. 3 and 4), which was further confirmed when overall gene expression variations of LPS-treated control and *Sfrp1-/-* microglia were plotted and compared (Fig. 7b, c). Linear regression analysis of this comparison demonstrated a 30% attenuation of the global response to LPS in the absence of *Sfrp1* (slope of red dotted line, Fig. 7d). LPS treatment in control microglia induced the upregulation of 1128

genes, 487 of which were shared with *Sfrp1*$_{-/-}$ microglia (Table S1-2). LPS treatment also induced the upregulation of 121 and the down-regulation of 167 microglial genes in the absence of SFRP1 (Fig. 7e; Table S2). Genes associated with metabolic pathways (i.e. *AldoA*, *LdhA* or *Pygl)*, the cell cycle (i.e. Gas6) or immune regulators (i.e. *Mif*, *Mefv*) were highly upregulated in controls but not in *Sfrp1*$_{-/-}$ microglia (Table S1), whereas genes downstream of the Toll-like 4 receptor (TLR4), such as *Tlr2,* were upregulated at similar levels in both genotypes (Table S1-2). TLR4 is fundamental for LPS recognition and the activation of the immediate inflammatory response (45), strongly suggesting that, in the absence of *Sfrp1*, microglial cells retain their prompt response to damage, as also shown by their cytokines' release upon LPS treatment (Fig. 6).

Consistent with this observation, hierarchical clustering of the samples demonstrated treatment-dependent similarities, but with *Sfrp1*$_{-/-}$ microglia showing an attenuated response to LPS treatment as compared to wt (Fig. 7f). Hierarchical clustering of the differentially expressed genes presented a pattern of covariance that was further analysed by Z-score covariance unsupervised clustering (Fig. 7f). This analysis generated 4 different clusters of upregulated genes, which were analysed for enrichment of regulatory elements and gene ontology annotations (Fig. 8). Genes regulated by E2F transcription factors and implicated in cell cycle regulation composed the less abundant 3 and 4 clusters. Genes belonging to cluster 3, involved in the regulation of chromosomal segregation and spindle organization, were slightly more upregulated in control microglia. On the contrary, genes belonging to cluster 4 and involved in chromatin assembly and DNA packing were upregulated in *Sfrp1*$_{-/-}$ microglia, suggesting possible differences in the length of the cell cycle (not shown).

One and 2 were the largest clusters and included genes that mediate the inflammatory response and regulators of the defence response (Fig. 8a, b). Both clusters were strongly upregulated in control microglia in response to LPS (Fig. 8a): genes in cluster 1 showed significant enrichment in NF-kB TF binding sites at the promoter regions, whereas those putatively controlled by Hif transcription factors were enriched in cluster 2 (Fig. 8c; Table S5-6). In microglia derived from *Sfrp1*$_{-/-}$ mice, the expression of a few genes belonging to cluster 1 was decreased (Fig. 8a, Table S5), whereas that of genes belonging to cluster 2 was basically abrogated (Fig. 8a, Table S6). Ingenuity Pathway Analysis network representation of the NF-κB and HIF downstream targets showed that in *Sfrp1* absence, the activity of both pathways was altered but with a higher impact on the HIF one (Fig, 9a). Genes downstream NF-κB, such as *Tlr2* and *ApoE* showed LPS-dependent up-regulation with levels almost similar in the two genotypes, whereas the expression of the homeostatic *Cx3cr1* and *Trem2* genes was unchanged

(Fig. 9b; Table S5). Of note, a number of genes shared between the NF-κB and HIF pathways, such as *Cxcl2*, *Cxcl3* and *Ptgs2*, were strongly up-regulated in LPS-treated control microglia but not in those derived from *Sfrp1*$^{-/-}$ brains (Fig. 9a). Similarly, other LPS-induced HIF targets failed to be up-regulated in the absence of *Sfrp1* and maintained levels of expression comparable to those of saline-treated control microglia (Fig. 9a, b; Table S6). These included *Vegfa*, *Sod2*, *Mif*, *Aldoa* and *Ldha*. Notably, Hif1α expression was similar to that observed in LPS treated controls (Table S6).

All in all, these results support the idea that in the absence of *Sfrp1* microglial cells can sense and respond to an inflammatory insult undertaking an initial response. SFRP1 is however required to enhance this response allowing for the full activation of microglial-mediated inflammation in the brain.

Discussion

Microglial cells transit from a surveying to an activated state in response to adverse signals derived from the surrounding environment (46). However, both insufficient or prolonged microglia activation is harmful to the brain so that an elaborated neuron-microglia-astrocyte cross talk is in charge of shaping the brain immune response to damage (47). The molecular components that mediate the flux of information from neurons to microglia (i.e. the CD200/ CD200R signalling system; (46) or from microglia to astrocytes (i.e. cytokines and NO; (2) have been in part identified. In contrast, there is perhaps less information on how astrocytes communicate with microglial cells (2). Our study unveils that SFRP1 is part of the molecular signals that astrocytes provide to microglial cells to enhance their inflammatory response. In response to damage, reactive astrocytes produce and secreted SFRP1, which, in turn, increases the number of activated microglial cells and fosters the expression of HIF and, to a much lower extent, NF-kB down-stream targets in microglial cells. Persistent SFRP1 up-regulation is however pernicious as it sustains a chronic inflammatory state. Indeed, its inactivation significantly reduces the prolonged neuroinflammation associated with EAE. These observations indicate that SFRP1 is a potential valuable target to counteract the harmful effect of prolonged inflammatory conditions, such as those present in MS or AD.

As an advantage, neutralization of SFRP1 function should have less effect on the initial acute inflammatory phase, which is a necessary step towards pathogen elimination, tissue repair and homeostasis restoration (47). Abrogation of SFRP1 function does not prevent this acute response given that, in its absence, both LPS-infusion and MOG-immunisation induce an initial inflammatory reaction, albeit at somewhat lower levels. Furthermore, activated microglial cells and infiltrated monocytes can still be isolated from the brain of *Sfrp1*$^{-/-}$ mice, although at significantly decreased numbers. These microglial cells retain phagocytic competence, although with a significant less efficiency and no significant difference was observed in the LPS-induced cytokines' release of purified microglial cells obtained from *Sfrp1*$^{-/-}$ and wt brains. This agrees with the observation that in homeostatic conditions SFRP1 is very poorly expressed in the adult mammalian brain (23) and this study). Our transcriptomic analysis shows that *Sfrp1*$^{-/-}$ microglia cells retain their capacity of sensing LPS, providing strong support to the implication of SFRP1 in the amplification of the inflammatory response. Indeed, *Tlr2* expression, a read-out of LPS-mediated TLR4 activation (37), is increased (and to a comparable extent) in microglial cells from both genotypes. A similar consideration applies to a large

fraction of the genes related to the NFκB-dependent pathway, which is largely related to the acute inflammatory response (25).

Brain response to LPS, but also to other harmful signals, depends on the fast reaction of functional microglial cells (48), whereas astrocytes and neurons do not initially and directly participate in this response despite their reported expression of the TLR4 receptor (49, 50). Reactive microglial cells thereafter induce astrocytes activation that, in turn, feeds back on microglial function (2). Fitting our data into this loop, we propose that up-regulation and release of SFRP1 from astrocytes occurs as part of their microglia-mediated early activation. Secreted SFRP1 then acts on microglial cells amplifying a HIF-dependent inflammatory response and thus a significant increase in cytokine secretion, further impinging upon inflammation. This implies that, as long as SFRP1 up-regulation persists, neuroinflammation persists, contributing to its chronicization. This idea is well in agreement with our observation that genetic inactivation of *Sfrp1* significantly limits the severity and progression of EAE, a condition that, as MS, is characterised by persistent microglial activation. Both EAE and MS are driven by the infiltration of peripheral macrophages and lymphocytes (51). We cannot exclude that the lack of peripherally expressed *Sfrp1* may limit this infiltration and thus the disease, especially because SFRP1 has been shown to influence lymphocytes' differentiation (52). Notwithstanding there is strong evidence that endogenous microglial activation is critical for EAE development and maintenance (53, 54) and the *SFRP1* gene is hypomethylated in brain samples from MS patients (55), likely promoting an abnormal protein increase. Thus, reduced microglial activation is a very plausible cause of the milder EAE symptoms observed in *Sfrp1*$^{-/-}$ mice.

SFRP1 up-regulation in other neurodegenerative diseases characterized by the presence of chronic inflammation further supports a role of SFRP1 microglial activation. An example is Glaucoma (56) or AD, in which antibody-mediated neutralization of SFRP1 strongly decreases different AD pathological features, including neuroinflammation (23). Notably, SFRP1-mediated inhibition of ADAM10, a metalloprotease responsible for non-amyloidogenic processing of APP, contributes to the generation of toxic amyloid peptides in AD patients, whereas SFRP1 deficiency decreases amyloid burden (23). Low neuroinflammation upon SFRP1 neutralization could therefore be secondary to this reduction (23). The present study shows that this is not necessarily the case as SFRP1 acts directly on microglial cells, suggesting that SFRP1 simultaneously impinges upon multiple pathological events in AD. A possible SFRP1-mediated activation of microglial cells in AD finds further support in our transcriptomic analysis that links SFRP1 with HIF signalling. A number of recent studies have shown that

microglial cells isolated from AD-like mouse models undergo important metabolic changes with the activation of the HIF pathway (57-59). Furthermore, *Hif1a* seems to be dysregulated in association with other genes genetically linked to AD risk, suggesting that HIF-1α may be detrimental in AD pathology (59).

The precise molecular interactions underlying SFRP1-mediated HIF pathway activation are at the moment an open question. Microglial cells express members of the ADAM family of metalloproteases (14) and SFRP1 effectively inhibits their enzymatic activity in cultured microglial cells (our own observations). Given that TREM2 is a proven substrate of ADAM10/17 (14), it seems plausible to postulate that SFRP1 may modulate the shedding of TREM2 on the surface of microglial cells. This shedding occurs, for example, in response to LPS induced activation of TLR4 (60, 61), thereby attenuating microglial activation (60). Notably, microglial cells deficient in TREM2 undergo only a partial and abortive activation and remain locked in an almost homeostatic state (62, 63). It is thus tempting to speculate that in SFRP1 absence enhanced shedding of TREM2 may reduce microglial activation as we have observed in *Sfrp1*$^{-/-}$ mice, whereas high SFRP1 levels, by interfering with ADAM function, may enhance TREM2 signalling. In addition (or alternatively), SFRP1 may interfere with ADAM10-mediated shedding of the neuronal ligands CX3CL1 and CD200 preventing the generation of their soluble forms (15, 16) and thus the activation of their respective microglial receptors, CX3CR1 and CD200R (35, 64). Unfortunately, lack of appropriate biochemical tools has prevented us from verifying these possibilities in our mouse models, leaving this question open for future studies.

In conclusion, we have shown that astrocyte-derived SFRP1 plays an important role in shaping microglia response to CNS damage, sustaining chronic neuroinflammation. This effect might not be limited to the brain, as SFRP1 upregulation has been reported in different pathological conditions associated with inflammation or fibrosis such as periodontitis, rheumatoid arthritis, uropathies or pulmonary emphysema (10, 65). Therefore, SFRP1 neutralization (23) represents a promising therapeutic avenue to treat a wide variety of chronic pathological conditions worth of being investigated further.

Methods

Animals. We used newborn and adult mice of both sexes unless otherwise indicated. All mice were maintained under specific pathogen–free conditions in the animal facilities of the CBMSO, in accordance with current national and European guidelines (Directive 2010/63/EU). All animal procedures were approved by the ethical committee of the institute and of the Comunidad Autónoma de Madrid. *Sfrp1*$_{-/-}$ mice were generated by inter-cross of the *Sfrp1*$_{-/-}$*;Sfrp2*$_{+/-}$ mice in a mixed 129/C57BL/6 background as described (11). The obtained mice were back-crossed at least four times with C57BL/6J to unify the background. Wild type (wt) animals were littermates selected from heterozygous crosses. Breeding pairs of *CX*$_3$*CR1::GFP* mice (35) were kindly provided by Prof. J Avila, CBMSO. Mice were further crossed with the *Sfrp1*$_{-/-}$ to obtain *CX*$_3$*CR1::GFP;Sfrp1*$_{-/-}$.

Brain stereotaxic LPS infusion. LPS or saline were infused into the brain parenchyma of 10-12 weeks-old male littermates from wt (C57BL/6J) and *Sfrp1*$_{-/-}$ or *CX*$_3$*CR1*$_{+/GFP}$ and *CX*$_3$*CR1*$_{+/GFP}$*;Sfrp1*$_{-/-}$ mice. Animals were anaesthetized with 4% Isoflurane (Forane, AbbVie Farmacéutica) vaporised into a sealed anaesthetic induction chamber (SurgiVet, Smiths Medical) and placed into a stereotaxic apparatus (Stoelting). Anaesthesia was maintained at 2.5% in 250ml/min oxygen flow. Delivery of saline (2.5µl) or LPS (5µg; Escherichia coli 0111:B4; Sigma Aldrich) was performed through a small skull window using a Quintessential Stereotaxic Injector (Stoelting) coupled to a 10µl syringe with a 34G needle (Hamilton) at the rate of 0.5µl/min. Injections were performed at the following bregma coordinates: 0.0mm A-P; -1.0 mm lateral, and -1.5mm D/V. Mice were let survive for three days and then sacrificed and processed for biochemical or histological analysis. Delivery of pHrodo Red *E.coli* BioParticles Conjugate (Molecular Probes) was performed with a similar procedure at -2.5 mm A-P; 0.0 mm lateral, and -2.3 mm D-V from bregma. Lentiviral vectors (2.5 µl), generated as described below, were delivered 0.5 mm A-P; 1.0 mm lateral and -2.3 mm D-V from bregma. Mice were let survive from one to five months and then analysed.

Lentiviral vector generation. Lentiviral vectors carrying IRES-*Gfp* or *Sfrp1*-IRES-*Gfp* were obtained by transient transfection of mycoplasma-free HEK-293T cells (66, 67). Cells were transfected employing a three-plasmids HIV-derived and VSV pseudotyped lentiviral system kindly provided by M.K. Collins, University College London, UK; A. Thrasher, Institute of Child Health, UK; and D. Trono, Ecole Polytechnique Fédérale de Lausanne, Switzerland. Culture supernatants were collected two and three days after transfection and ultra-centrifuged

to concentrate vector particles. The pellets containing the lentiviral vectors were re-suspended in PBS and their functional titer was calculated on HEK-293T cells (1×10^8 TU/ml).

Experimental Autoimmune Encephalomyelitis (EAE). Chronic EAE was induced as described (42). Briefly, 8 to 10 weeks-old female C57BL/6J and *Sfrp1*$^{-/-}$ littermates were injected bilaterally in subcutaneous femoral region with 150 mg of MOG35–55 (Espikem) emulsified with Freund's complete adjuvant (Sigma Aldrich), supplemented with Mycobacterium tuberculosis (1mg/ml; H37Ra strain from Difco), followed by two intraperitoneal injections of pertussis toxin (200 ng; Sigma Aldrich) separated by 48 h. An observer blind to the animals' genotype weighed and inspected the animals daily to detect the appearance of clinical signs according to the following classification: 0) no overt signs of disease; 1) weakness at the distal portion of the tail; 1.5) complete tail flaccidity; 2) moderate hind limb weakness; 2.5) severe hind limb weakness; 3) ataxia; 3.5) partial hind limb paralysis; 4) complete hind limb paralysis; 4.5) complete hind limb paralysis with muscle stiffness; 5) moribund state and hence sacrificed according to ethical procedures. A representative pool of mice was anesthetized and perfused intracardially sixteen days after immunization, when symptoms were at their pick, for histological analysis. Other animals were let recover. Spinal cords were dissected and processed.

Primary cultures. Glial primary cultures were established from cerebral cortices of C57BL/6J or *Sfrp1*$^{-/-}$ 1-3 days-old pups dissected in Ca2+ and Mg2+ free Hank's Balanced Salt Solution (HBSS, Invitrogen) and processed following standard procedures (68). Cells were plated in Dulbecco's modified Eagle medium and F-12 nutrient mixture (DMEM/F12, Invitrogen) containing 10% Fetal Calf Serum (FCS, Invitrogen), and gentamycin (Sigma Aldrich). Cortices from two pups were platted in a 75cm^2 flask pre-treated with Poly-D-Lys (P7280, Sigma Aldrich) and cultured at 37ºC in a humidified 5% CO_2 incubator. The next day, the medium was replaced with fresh one containing 10% conditioned medium from the m-CSF1 secreting L929 cell line to improve microglial survival. Cultures were let reaching confluency (about 2 weeks) without further changes. For the analysis of mixed cultures, cell cultures were detached by washing with warm phosphate buffer saline (PBS), and then incubated with 0.25% trypsin (Invitrogen), 1mM EDTA in PBS at 37ºC for 15min. After the addition of DMEM/F12 supplemented with 10% FCS, cells were centrifuged for 5 min at 1000 rpm, and re-suspended in DMEM/F12 10% FCS.

Purified microglial cultures were obtained by mechanical detachment of mixed glial cultures, followed by medium centrifugation (5 min; 1000 rpm; (68) and 50% of the medium was

replaced to maintain an active proliferation of microglial cells. For analysis, cells were seeded on multi-well culture plates (Falcon) at a density of 10^5 cells/cm^2, let settle for 48 h and then treated with either LPS (1µg/ml; L3024, Sigma Aldrich) or human recombinant SFRP1 protein (0.5µg/ml; SRP3154 Sigma Aldrich). After treatment, cell media were collected and maintained at -80ºC until processed.

Immunohistochemistry and immunocytochemistry. New born and adult mice were transcardially perfused with 4% PFA in phosphate buffer 0.1M (wt/vol). Brains were removed, post-fixed by immersion overnight and then washed for 1 day in PBS, on a rocking platform at 4ºC. Spinal cords were extracted after whole body post-fixation and washing. Tissues were then incubated in a 30% sucrose-PB solution (wt/vol) for 24 h, embedded in a 7.5% gelatin; 15% sucrose solution (wt/vol), frozen on dry ice and, if necessary, stored at -80ºC until serially sectioned in the coronal plane at 15µm of thickness using a cryostat (Leica). Both histological and cytological immunostaining were performed following standard protocols, after antigen retrieval (10mM citrate buffer, pH6, for 5 min at 110ºC in a boiling chamber, BIOCAREMEDICAL). Primary antibodies, listed in Table S7, were incubated overnight at RT for immunohistochemistry and at 4ºC on a rocking platform for immunocytochemistry. The following secondary antibodies were incubated for 1h at RT: Alexa488 or Alexa594 conjugated donkey anti-rabbit (1:1000) and anti-mouse; Alexa488 or Alexa594 conjugated goat anti-rat (1:3000; Molecular Probes, Invitrogen) or anti-chicken, (1:2000, AbCAM); biotin conjugated goat anti-mouse or anti-rabbit (1:500, Jackson Lab). Alexa488 or Alexa594 (1:500; Molecular Probes, Invitrogen) or POD conjugated (Jackson Lab) streptavidin followed reaction with 3,3-diaminobenzidine (0.05%; Sigma) and 0.03% H_2O_2. For immunofluorescence, sections were counterstained with Hoechst (Sigma Aldrich). Sections were analysed with a DMCTR5000 microscope equipped with a DFC350Fx monochrome camera or a DFC500 colour camera (Leica Microsystems) or with a LSM710 confocal imaging system coupled to a AxioImager.M2 vertical microscope (Zeiss) or a LSM800 coupled to an Axio Observer inverted microscope (Zeiss). Fluorescence was quantified with ImageJ software (National Institute of Health).

ELISA. The cytokines' content present in the media glial cell cultures was quantified with electro-chemo-luminescence in a MSD MULTI-SPOT Assay System using 96 well V-PLEX plates for pro-inflammatory mouse panel 1 or custom mouse cytokine V-PLEX plates for IFNγ, IL1β, IL4, IL6, IL10 and TNFα (Meso Scale Discovery), following the manufacturer's indications and using a SECTOR Imager 2400 reader (Meso Scale Discovery). SFRP1 present in glial cell culture medium or in the RIPA fraction of brain lysates was determined with a

described capture ELISA (23). Culture media were diluted five folds, and brain lysates used at 0.1 µg/µl protein concentration determined with BCA protein assay (Thermo Scientific). Values were determined at 450 nm wave length using a FLUOstar OPTIMA microtiter plate reader (BMG LABTECH).

Fluorescence Activated Cell Sorting (FACS) and Flow Cytometry Analysis. *CX3CR1+/GFP* and *CX3CR1+/GFP;Sfrp1-/-* male littermates of 10-12 weeks of age were treated with LPS or saline as already described. After 3 days, animals were perfused with ice-cold saline and brains collected on ice-cold Hank's Balanced Salt Solution, Ca^{2+}, Mg^{2+}-free (HBSS, Invitrogen). After meninges' removal, cortices were isolated, finely chopped and digested in DMEM with GlutMAX (Invitrogen) containing papain 20U/ml (Worthington Biochemical Corporation), DNase (50U/ml, Sigma Aldrich) and L-Cysteine (1mM, MERCK) for 20 min. After addition of 20% FCS (Invitrogen), the tissue was mechanically dissociated and filtered on a 35µm nylon strainer (Falcon). Microglial cells were separated from myelin and debris by Isotonic Percoll gradient centrifugation (35% Fisher Scientific) at 2000 rpm for 45min at 4ºC. The cell pellet was recovered and sequentially incubated with anti-mouse CD16/CD32 (1:250, BD Pharmingen) in 2% BSA, 5mM EDTA in PBS for 15min at 4ºC, followed by rat anti-CD11b and PerCP-Cy5.5 rat anti-mouse CD45 (1:200, BD Pharmingen) in the same solution for 30min at 4ºC. After washing, the cells were sorted using a BD FACS Aria Fusion Flow Cytometer and their fluorescence, size and complexity acquired with DiVA8 Software (BD Pharmingen). Analysis was performed using FlowJo v10.0.7 Software (BD Pharmingen).

Genomic Data Processing and Access. RNA from sorted microglia was extracted with the TRI reagent (MERCK) according to the manufacturer's instructions, purified with RNeasy Lipid Mini Kit (Qiagen) following the manufacturer's protocol and the resulting total RNA was treated with RNase-Free DNase Set (Qiagen). RNA quality was assessed with a Bioanalyzer 2100 system (Aligent), obtaining RIN (RNA integrity number) values between 8.8 and 10. Each sample, composed of microglia sorted from a single mouse brain, was processed to obtain a RiboZero Stranded Gold Library (Illumina) and sequenced in HiSeq 4000 sequencer in paired-end configuration with 150bp sequence reads (Illumina). Sequence quality was determined with FastQC (Babraham Bioinformatics) revealing more than 32 million mean cluster reads of over 38 quality score and 93% mean Q30. Reads were aligned with HISAT2 v2.1.0 (69) to Ensemble *Mus musculus* (GRCm38.94). Aligned reads were further processed using Samtools v1.9 (70) and quantified to gene level using HTseq v0.11.2 (71). Whole genome alignments were visualized with Integrative Genomics Viewer (IGV v2.5; (72). Differential expression analysis

(DGE) was performed using the Bioconductor package DESeq2 v1.10.0 (73). DGE data were processed with custom R scripts (R version 3.5.1, 2018) considering genes with adjusted p-value < 0.05 and log2 Fold Change > +/- 0.8 as significantly up- or down-regulated. Analysis of GO terms was performed with the Bioconductor package clusterProfiler (74) and that of promoter-based motif enrichment with HOMER (75). Genomic data sets can be accessed at the European Nucleotide Archive public repository under the following accession numbers (ERP119668 / PRJEB3647).

Statistical analysis was performed using Prism v7 software (GraphPad). Different statistical test were used as indicated in each figure footnote and represented by *P<0.05, **P<0.01, ***P<0.001, ****P<0.0001.

Author contributions

JRC, PE and PB conceptualized and designed the research study. JRC, MIM and MJMB conducted the experiments and acquired the data. AB, JRC and BA designed, the EAE study and JRC and AB conducted and analyzed it. JRC, MIM, MTH, PE and PB analyzed the data. MPK and SS provided support with cytokine analysis. JRC and PB wrote the paper. JPLA supervised RNAseq analysis. All authors read and approved the manuscript.

Acknowledgements

We wish to thank J Avila, CBM, for providing a breading pair of the *CX3CR1::GFP* mice and the CBM image analysis, genomic and cytometry facilities for their support and advices during the course of this study. This work was supported by grants from the Spanish MINECO (BFU2013-43213-P; BFU2016-75412-R with FEDER support), Fundación Tatiana Perez de Guzman el Bueno and CIBERER to PB and PE. JRC (BES-2011-047189) and MIM (BES-2014-068797) were supported by FPI fellowships from the MINECO. We also acknowledge a CBM Institutional grant from the Fundación Ramon Areces.

References

1. Marinelli S, Basilico B, Marrone MC, and Ragozzino D. Microglia-neuron crosstalk: Signaling mechanism and control of synaptic transmission. *Semin Cell Dev Biol.* 2019.
2. Jha MK, Jo M, Kim JH, and Suk K. Microglia-Astrocyte Crosstalk: An Intimate Molecular Conversation. *Neuroscientist.* 2019;25(3):227-40.
3. Ransohoff RM. How neuroinflammation contributes to neurodegeneration. *Science.* 2016;353(6301):777-83.
4. Escartin C, Guillemaud O, and Carrillo-de Sauvage MA. Questions and (some) answers on reactive astrocytes. *Glia.* 2019.
5. Frank-Cannon TC, Alto LT, McAlpine FE, and Tansey MG. Does neuroinflammation fan the flame in neurodegenerative diseases? *Mol Neurodegener.* 2009;4:47.
6. Perry VH, and Holmes C. Microglial priming in neurodegenerative disease. *Nat Rev Neurol.* 2014;10(4):217-24.
7. Glass CK, Saijo K, Winner B, Marchetto MC, and Gage FH. Mechanisms underlying inflammation in neurodegeneration. *Cell.* 2010;140(6):918-34.
8. Sarlus H, and Heneka MT. Microglia in Alzheimer's disease. *J Clin Invest.* 2017;127(9):3240-9.
9. Hickman S, Izzy S, Sen P, Morsett L, and El Khoury J. Microglia in neurodegeneration. *Nat Neurosci.* 2018;21(10):1359-69.
10. Esteve P, and Bovolenta P. The advantages and disadvantages of sfrp1 and sfrp2 expression in pathological events. *Tohoku J Exp Med.* 2010;221(1):11-7.
11. Esteve P, Sandonis A, Cardozo M, Malapeira J, Ibanez C, Crespo I, et al. SFRPs act as negative modulators of ADAM10 to regulate retinal neurogenesis. *Nat Neurosci.* 2011;14(5):562-9.
12. Saftig P, and Lichtenthaler SF. The alpha secretase ADAM10: A metalloprotease with multiple functions in the brain. *Prog Neurobiol.* 2015;135:1-20.
13. Lichtenthaler SF, Lemberg MK, and Fluhrer R. Proteolytic ectodomain shedding of membrane proteins in mammals-hardware, concepts, and recent developments. *EMBO J.* 2018;37(15).
14. Kleinberger G, Yamanishi Y, Suarez-Calvet M, Czirr E, Lohmann E, Cuyvers E, et al. TREM2 mutations implicated in neurodegeneration impair cell surface transport and phagocytosis. *Sci Transl Med.* 2014;6(243):243ra86.
15. Hundhausen C, Schulte A, Schulz B, Andrzejewski MG, Schwarz N, von Hundelshausen P, et al. Regulated Shedding of Transmembrane Chemokines by the Disintegrin and Metalloproteinase 10 Facilitates Detachment of Adherent Leukocytes. *The Journal of Immunology.* 2007;178(12):8064-72.
16. Wong KK, Zhu F, Khatri I, Huo Q, Spaner DE, and Gorczynski RM. Characterization of CD200 Ectodomain Shedding. *PLoS One.* 2016;11(4):e0152073.
17. Musardo S, Marcello E, Gardoni F, and Di Luca M. ADAM10 in synaptic physiology and pathology. *Neurodegener Dis.* 2014;13(2-3):72-4.
18. Prox J, Bernreuther C, Altmeppen H, Grendel J, Glatzel M, D'Hooge R, et al. Postnatal disruption of the disintegrin/metalloproteinase ADAM10 in brain causes epileptic seizures, learning deficits, altered spine morphology, and defective synaptic functions. *J Neurosci.* 2013;33(32):12915-28, 28a.
19. Suh J, Choi SH, Romano DM, Gannon MA, Lesinski AN, Kim DY, et al. ADAM10 missense mutations potentiate beta-amyloid accumulation by impairing prodomain chaperone function. *Neuron.* 2013;80(2):385-401.
20. Kunkle BW, Grenier-Boley B, Sims R, Bis JC, Damotte V, Naj AC, et al. Genetic meta-analysis of diagnosed Alzheimer's disease identifies new risk loci and implicates Abeta, tau, immunity and lipid processing. *Nat Genet.* 2019;51(3):414-30.
21. Kuhn PH, Wang H, Dislich B, Colombo A, Zeitschel U, Ellwart JW, et al. ADAM10 is the physiologically relevant, constitutive alpha-secretase of the amyloid precursor protein in primary neurons. *EMBO J.* 2010;29(17):3020-32.
22. Marcello E, Borroni B, Pelucchi S, Gardoni F, and Di Luca M. ADAM10 as a therapeutic target for brain diseases: from developmental disorders to Alzheimer's disease. *Expert Opin Ther Targets.* 2017;21(11):1017-26.

23. Esteve P, Rueda-Carrasco J, Ines Mateo M, Martin-Bermejo MJ, Draffin J, Pereyra G, et al. Elevated levels of Secreted-Frizzled-Related-Protein 1 contribute to Alzheimer's disease pathogenesis. *Nat Neurosci.* 2019;22(8):1258-68.
24. Helton R, Cui J, Scheel JR, Ellison JA, Ames C, Gibson C, et al. Brain-specific knock-out of hypoxia-inducible factor-1alpha reduces rather than increases hypoxic-ischemic damage. *J Neurosci.* 2005;25(16):4099-107.
25. Kaltschmidt B, and Kaltschmidt C. NF-kappaB in the nervous system. *Cold Spring Harb Perspect Biol.* 2009;1(3):a001271.
26. Esteve P, Crespo I, Kaimakis P, Sandonis A, and Bovolenta P. Sfrp1 Modulates Cell-signaling Events Underlying Telencephalic Patterning, Growth and Differentiation. *Cereb Cortex.* 2019;29(3):1059-74.
27. Esteve P, Sandonis A, Ibanez C, Shimono A, Guerrero I, and Bovolenta P. Secreted frizzled-related proteins are required for Wnt/beta-catenin signalling activation in the vertebrate optic cup. *Development.* 2011;138(19):4179-84.
28. Campanelli JT, Sandrock RW, Wheatley W, Xue H, Zheng J, Liang F, et al. Expression profiling of human glial precursors. *BMC Dev Biol.* 2008;8:102.
29. Augustine C, Gunnersen J, Spirkoska V, and Tan SS. Place- and time-dependent expression of mouse sFRP-1 during development of the cerebral neocortex. *Mech Dev.* 2001;109(2):395-7.
30. Zhang Y, Sloan SA, Clarke LE, Caneda C, Plaza CA, Blumenthal PD, et al. Purification and Characterization of Progenitor and Mature Human Astrocytes Reveals Transcriptional and Functional Differences with Mouse. *Neuron.* 2016;89(1):37-53.
31. Folke J, Pakkenberg B, and Brudek T. Impaired Wnt Signaling in the Prefrontal Cortex of Alzheimer's Disease. *Mol Neurobiol.* 2019;56(2):873-91.
32. Youm YH, Grant RW, McCabe LR, Albarado DC, Nguyen KY, Ravussin A, et al. Canonical Nlrp3 inflammasome links systemic low-grade inflammation to functional decline in aging. *Cell Metab.* 2013;18(4):519-32.
33. Blalock EM, Geddes JW, Chen KC, Porter NM, Markesbery WR, and Landfield PW. Incipient Alzheimer's disease: microarray correlation analyses reveal major transcriptional and tumor suppressor responses. *Proc Natl Acad Sci U S A.* 2004;101(7):2173-8.
34. Wright SD. Toll, a new piece in the puzzle of innate immunity. *J Exp Med.* 1999;189(4):605-9.
35. Jung S, Aliberti J, Graemmel P, Sunshine MJ, Kreutzberg GW, Sher A, et al. Analysis of fractalkine receptor CX(3)CR1 function by targeted deletion and green fluorescent protein reporter gene insertion. *Mol Cell Biol.* 2000;20(11):4106-14.
36. Satoh W, Gotoh T, Tsunematsu Y, Aizawa S, and Shimono A. Sfrp1 and Sfrp2 regulate anteroposterior axis elongation and somite segmentation during mouse embryogenesis. *Development.* 2006;133(6):989-99.
37. Rivest S. Regulation of innate immune responses in the brain. *Nat Rev Immunol.* 2009;9(6):429-39.
38. Mii Y, and Taira M. Secreted Frizzled-related proteins enhance the diffusion of Wnt ligands and expand their signalling range. *Development.* 2009;136(24):4083-8.
39. Heneka MT, Kummer MP, and Latz E. Innate immune activation in neurodegenerative disease. *Nat Rev Immunol.* 2014;14(7):463-77.
40. Ising C, Venegas C, Zhang S, Scheiblich H, Schmidt SV, Vieira-Saecker A, et al. NLRP3 inflammasome activation drives tau pathology. *Nature.* 2019;575(7784):669-73.
41. Constantinescu CS, Farooqi N, O'Brien K, and Gran B. Experimental autoimmune encephalomyelitis (EAE) as a model for multiple sclerosis (MS). *Br J Pharmacol.* 2011;164(4):1079-106.
42. Borroto A, Reyes-Garau D, Jimenez MA, Carrasco E, Moreno B, Martinez-Pasamar S, et al. First-in-class inhibitor of the T cell receptor for the treatment of autoimmune diseases. *Sci Transl Med.* 2016;8(370):370ra184.
43. Greter M, Lelios I, and Croxford AL. Microglia Versus Myeloid Cell Nomenclature during Brain Inflammation. *Front Immunol.* 2015;6:249.
44. Kapellos TS, Taylor L, Lee H, Cowley SA, James WS, Iqbal AJ, et al. A novel real time imaging platform to quantify macrophage phagocytosis. *Biochem Pharmacol.* 2016;116:107-19.

45. Ransohoff RM, and Perry VH. Microglial physiology: unique stimuli, specialized responses. *Annu Rev Immunol.* 2009;27:119-45.
46. Kierdorf K, and Prinz M. Factors regulating microglia activation. *Front Cell Neurosci.* 2013;7:44.
47. Colonna M, and Butovsky O. Microglia Function in the Central Nervous System During Health and Neurodegeneration. *Annu Rev Immunol.* 2017;35:441-68.
48. Holm TH, Draeby D, and Owens T. Microglia are required for astroglial Toll-like receptor 4 response and for optimal TLR2 and TLR3 response. *Glia.* 2012;60(4):630-8.
49. Bowman CC, Rasley A, Tranguch SL, and Marriott I. Cultured astrocytes express toll-like receptors for bacterial products. *Glia.* 2003;43(3):281-91.
50. Rolls A, Shechter R, London A, Ziv Y, Ronen A, Levy R, et al. Toll-like receptors modulate adult hippocampal neurogenesis. *Nat Cell Biol.* 2007;9(9):1081-8.
51. Ajami B, Bennett JL, Krieger C, McNagny KM, and Rossi FM. Infiltrating monocytes trigger EAE progression, but do not contribute to the resident microglia pool. *Nat Neurosci.* 2011;14(9):1142-9.
52. Lee YS, Lee KA, Yoon HB, Yoo SA, Park YW, Chung Y, et al. The Wnt inhibitor secreted Frizzled-Related Protein 1 (sFRP1) promotes human Th17 differentiation. *Eur J Immunol.* 2012;42(10):2564-73.
53. Becher B, Durell BG, Miga AV, Hickey WF, and Noelle RJ. The clinical course of experimental autoimmune encephalomyelitis and inflammation is controlled by the expression of CD40 within the central nervous system. *J Exp Med.* 2001;193(8):967-74.
54. Heppner FL, Greter M, Marino D, Falsig J, Raivich G, Hovelmeyer N, et al. Experimental autoimmune encephalomyelitis repressed by microglial paralysis. *Nat Med.* 2005;11(2):146-52.
55. Chomyk AM, Volsko C, Tripathi A, Deckard SA, Trapp BD, Fox RJ, et al. DNA methylation in demyelinated multiple sclerosis hippocampus. *Sci Rep.* 2017;7(1):8696.
56. Wang WH, McNatt LG, Pang IH, Millar JC, Hellberg PE, Hellberg MH, et al. Increased expression of the WNT antagonist sFRP-1 in glaucoma elevates intraocular pressure. *J Clin Invest.* 2008;118(3):1056-64.
57. Baik SH, Kang S, Lee W, Choi H, Chung S, Kim JI, et al. A Breakdown in Metabolic Reprogramming Causes Microglia Dysfunction in Alzheimer's Disease. *Cell Metab.* 2019;30(3):493-507 e6.
58. Ulland TK, Song WM, Huang SC, Ulrich JD, Sergushichev A, Beatty WL, et al. TREM2 Maintains Microglial Metabolic Fitness in Alzheimer's Disease. *Cell.* 2017;170(4):649-63 e13.
59. Wendeln AC, Degenhardt K, Kaurani L, Gertig M, Ulas T, Jain G, et al. Innate immune memory in the brain shapes neurological disease hallmarks. *Nature.* 2018;556(7701):332-8.
60. Turnbull IR, Gilfillan S, Cella M, Aoshi T, Miller M, Piccio L, et al. Cutting Edge: TREM-2 Attenuates Macrophage Activation. *The Journal of Immunology.* 2006;177(6):3520-4.
61. Piccio L, Buonsanti C, Mariani M, Cella M, Gilfillan S, Cross AH, et al. Blockade of TREM-2 exacerbates experimental autoimmune encephalomyelitis. *Eur J Immunol.* 2007;37(5):1290-301.
62. Keren-Shaul H, Spinrad A, Weiner A, Matcovitch-Natan O, Dvir-Szternfeld R, Ulland TK, et al. A Unique Microglia Type Associated with Restricting Development of Alzheimer's Disease. *Cell.* 2017;169(7):1276-90 e17.
63. Mazaheri F, Snaidero N, Kleinberger G, Madore C, Daria A, Werner G, et al. TREM2 deficiency impairs chemotaxis and microglial responses to neuronal injury. *EMBO Rep.* 2017;18(7):1186-98.
64. Wright GJ, Puklavec MJ, Willis AC, Hoek RM, Sedgwick JD, Brown MH, et al. Lymphoid/neuronal cell surface OX2 glycoprotein recognizes a novel receptor on macrophages implicated in the control of their function. *Immunity.* 2000;13(2):233-42.
65. Claudel M, Jouzeau JY, and Cailotto F. Secreted Frizzled-related proteins (sFRPs) in osteo-articular diseases: much more than simple antagonists of Wnt signaling? *FEBS J.* 2019.
66. Marin V, Stornaiuolo A, Piovan C, Corna S, Bossi S, Pema M, et al. RD-MolPack technology for the constitutive production of self-inactivating lentiviral vectors pseudotyped with the nontoxic RD114-TR envelope. *Mol Ther Methods Clin Dev.* 2016;3:16033.
67. Merten OW, Hebben M, and Bovolenta C. Production of lentiviral vectors. *Mol Ther Methods Clin Dev.* 2016;3:16017.
68. Bovolenta P, Wandosell F, and Nieto-Sampedro M. Neurite outgrowth inhibitors associated with glial cells and glial cell lines. *Neuroreport.* 1993;5(3):345-8.

69. Kim D, Paggi JM, Park C, Bennett C, and Salzberg SL. Graph-based genome alignment and genotyping with HISAT2 and HISAT-genotype. *Nat Biotechnol.* 2019;37(8):907-15.
70. Li H, Handsaker B, Wysoker A, Fennell T, Ruan J, Homer N, et al. The Sequence Alignment/Map format and SAMtools. *Bioinformatics.* 2009;25(16):2078-9.
71. Anders S, Pyl PT, and Huber W. HTSeq--a Python framework to work with high-throughput sequencing data. *Bioinformatics.* 2015;31(2):166-9.
72. Thorvaldsdottir H, Robinson JT, and Mesirov JP. Integrative Genomics Viewer (IGV): high-performance genomics data visualization and exploration. *Brief Bioinform.* 2013;14(2):178-92.
73. Love MI, Huber W, and Anders S. Moderated estimation of fold change and dispersion for RNA-seq data with DESeq2. *Genome Biol.* 2014;15(12):550.
74. Yu G, Wang LG, Han Y, and He QY. clusterProfiler: an R package for comparing biological themes among gene clusters. *OMICS.* 2012;16(5):284-7.
75. Heinz S, Benner C, Spann N, Bertolino E, Lin YC, Laslo P, et al. Simple combinations of lineage-determining transcription factors prime cis-regulatory elements required for macrophage and B cell identities. *Mol Cell.* 2010;38(4):576-89.

Figure legends

Figure 1. Astrocytes upregulate SFRP1 expression upon LPS stimulation. a, b) Confocal image analysis of cryostat sections from adult *CX3CR1+/GFP;Sfrp1+/βgal* mouse brains three days after intra-cortical infusion of saline or LPS. Sections were immunostained for βgal (magenta) and Iba1 (green, a) or Sfrp1 (magenta) and GFP (green, b), and GFAP (cyan). Arrowheads indicate βgal/GFAP (a) and Sfrp1/GFP colocalization (b). Scale bar 25µm. c) ELISA quantification of SFRP1 levels present in extracts from 10 mm^3 cortical cubes isolated from the region abutting the injection site (n=5 mice for each group). Error bars represent Standard Error. Statistical significance: ****P<0.0001 by two-sided Student's t-test.

Figure 2. **LV-mediated *Sfrp1* gene addition suffices to promote glial cell activation.** a) Diagram of the observed GFP distribution (green dots) after lentiviral (LV)-particles' delivery into the lateral ventricle (*Lv*). Fluorescent GFP signal was no longer visible, unless detected with immunohistochemistry. b) Coronal cryostat sections of LV-IRES-*Gfp* or LV-*Sfrp1*-IRES-*Gfp* infected brains 1-month post-infusion, immunostained for SFRP1 (green) GFAP, Iba1 or TauP (red). c) The graph shows the level of GFAP, Iba1 and CD45 immunoreactivity (IR) and the area occupied by TauP signal (n=24 acquisitions; N=3 mice for each group), normalized to LV-*IRES-Gfp* infected brains. Error bars represent Standard Error. Statistical significance: ****P<0.0001 by two-sided Student's t-test. d) Coronal sections from LV-*IRES-Gfp* or LV-*Sfrp1-IRES-Gfp* infected brains 1 or 5 months (m) post-infusion (PI). Sections were immunostained for CD45. Arrowheads indicate $CD45^{hi}$-positive macrophages or lymphocytes infiltrated in the parenchyma after prolonged LV-*Sfrp1-IRES-Gfp* infection. High power images 1 and 2 were taken from the regions indicated with grey dotted lines in A. Scale bar 100µm.

Figure 3. **SFRP1 is required to enhance glial cell activation upon LPS treatment.** a,b) Coronal sections from wt and *Sfrp1-/-* animals 3 days after infusion of saline or LPS, immunostained for GFAP (cyan, a) or CD45 (magenta, b). Scale bar 60µm. c,d) The graphs show the levels of immunoreactivity (IR) for GFAP (c) and CD45 (d, P=0,006) present in cortical sections (n=24 acquisitions from N=3 animals per group) from WT and *Sfrp1-/-* animals infused with saline or LPS. Error bars represent Standard Error. Statistical significance: ** or ## P<0.01, **** or #### P<0.0001 by two-way ANOVA followed by Bonferroni's multiple comparisons test. * and # indicate significance between genotypes and treatments, respectively.

Figure 4. *Sfrp1*$_{-/-}$ mice develop a milder form of EAE. a) Time course analysis of the symptoms (extreme, plum; major, red; moderate, orange; mild, yellow; none, green) in wt and Sfrp1$_{-/-}$ mice after EAE induction. Data are expressed as % of the total number of analysed animals (n=19 per genotype). b) Wt and *Sfrp1*$_{-/-}$ mice immunised with MOG and sacrificed 16 days post immunization. Cryostat sections of the thoracic spinal cords were stained with antibodies against CD4, Iba1, GFAP and MBP. Images show the region dorsal fasciculus. Scale bar 200µm. c) Quantification of CD4+ infiltrated lymphocytes, Iba1 immunoreactivity and MBP immunoreactive area in the dorsal fasciculus of spinal cord sections from wt and *Sfrp1*$_{-/-}$ mice 16 days after immunisation (n=16 acquisitions from N=4 animals per genotype). Statistical significance: *P<0.05, **P<0.01, ***P<0.001 by Kolmogorov-Smirnov test followed by Mann–Whitney U nonparametric test comparing mice of same day after immunization (a) or two-sided Student's t-test (c).

Figure 5. *Sfrp1* amplifies LPS-induced microglial activation. a) Representative cytometry plots of CD11b+ populations present in the cortex of *CX$_3$CR1$_{GFP/+}$* or *CX$_3$CR1$_{GFP/+}$;Sfrp1$_{-/-}$* mice 3 days after saline or LPS intraventricular infusion. Gating was set for isolating the following myeloid cell populations: CD11b$_+$;CD45$_{lo}$;GFP$_+$ surveying microglia, CD11b$_+$;CD45$_+$;GFP$_+$ activated microglia and CD11b$_+$;CD45$_+$;GFP$_-$ infiltrated monocytes. b) Quantification of the percentage of activated microglia and infiltrated monocyte present in *Sfrp1*$_{-/-}$ and controls brains 3 days after infusion of saline or LPS. c) Quantification of the total fluorescence from engulfed pHrodo-labelled *E. coli* bioparticles and percentage of phagocyting cells in the CD11b$_+$;GFP$_+$ microglial population. Error bars represent Standard Error. Statistical significance: **P<0.01, ***P<0.001 by two-way ANOVA followed by Bonferroni's multiple comparisons test.

Figure 6. **Astrocyte-derived SFRP1 modifies cytokine secretion from activated microglia.** Secretory profile of cytokine present in the medium of primary microglia or microglia and astrocytes cultures from wt and *Sfrp1*$_{-/-}$ pups exposed for 24h to saline or LPS (1µg/ml). The culture media content of IFNγ, TNFα, IL1β, IL4, IL6 and IL10 was determined by ELISA. Values, normalised to those of untreated wt cultures, are represented in Log scale. Error bars represent Standard Error. Statistical significance: ns P>0.05, *P<0.05,***P<0.001, ****P<0.0001 by two-way ANOVA followed by Bonferroni's multiple comparisons test.

Figure 7. *Sfrp1* enhances the transcriptional response of microglial cells to LPS treatment. a) Principal component analysis with the 1000 most variable genes from microglial cells

isolated from *CX3CR1GFP/+* and *CX3CR1GFP/+;Sfrp1-/-* mouse brains three days after saline or LPS intra-cerebroventricular infusion. The analysis depicts sample clusterization by genotype and treatment. b, c) Volcano plots of differential gene expression from *CX3CR1GFP/+* (b) or *CX3CR1GFP/+;Sfrp1-/-* (c) microglial cell in response to LPS. Data are represented as Log2 Fold Change vs -Log10 adjusted p-value. Blue vertical lines represent an increase of 75 and 400% in the expression levels respectively. Green horizontal lines represent a 0.05 or 0.01 adjusted p-value of statistical significance respectively. d) Scatterplot of differential expressed genes in *CX3CR1GFP/+* and *CX3CR1GFP/+;Sfrp1-/-* microglia; the red line represents linear regression (slope 0.704014 p-value: < 2.2e-16) of the differential expression, indicating response attenuation. Coloured dots represent response which are exclusive for each genotype as represented in e. e) Venn diagram showing the extent of differential gene expression between *CX3CR1GFP/+* and *CX3CR1GFP/+;Sfrp1-/-* microglial cells. Fold change (75%) and adjusted p-value < 0.05 cut-off. f) Heatmap showing fold changes of regularized log transformed gene-level RNA-seq counts with hierarchical clustering of samples and differentially expressed genes

Figure 8. Sfrp1 promotes microglial inflammatory response dependent on HIF factors. a) Representation of the two principal k-means unsupervised clusters of upregulated genes in response to LPS in *CX3CR1GFP/+* or *CX3CR1GFP/+;Sfrp1-/-* microglial cells. Eight different clusters were generated by Z-scores covariation. The clusters are indicated in the heatmap of Fig.7f. b) Gene Ontology Enrichment Analysis of different clusters, GO biological process annotated are represented by fold enrichment and color-coded by adjusted p-value of enrichment and number of genes of each cluster in that term. c) Regulatory Elements Analysis of different clusters. Specifically-enriched transcription factors are represented by fold enrichment relative to the overall transcripts present in the microglia transcriptome. Coloured by Log odds detection threshold and the percentage of total targets for each transcription factor present in the cluster.

Figure 9. Sfrp1 induces the upregulation of HIF target genes during neuroinflammation. a) Ingenuity Pathway Analysis network representation of NF-κB and HIF downstream targets for *CX3CR1GFP/+* and *CX3CR1GFP/+;Sfrp1-/-* microglial cells. Coloured by Z-score alteration of their expression after LPS stimulus. b) Integrative Genomics Viewer transcription profile of represented genes for saline and LPS treatments of *CX3CR1GFP/+* and *CX3CR1GFP/+;Sfrp1-/-* microglial cells. Scale bar: 2 Kbp.

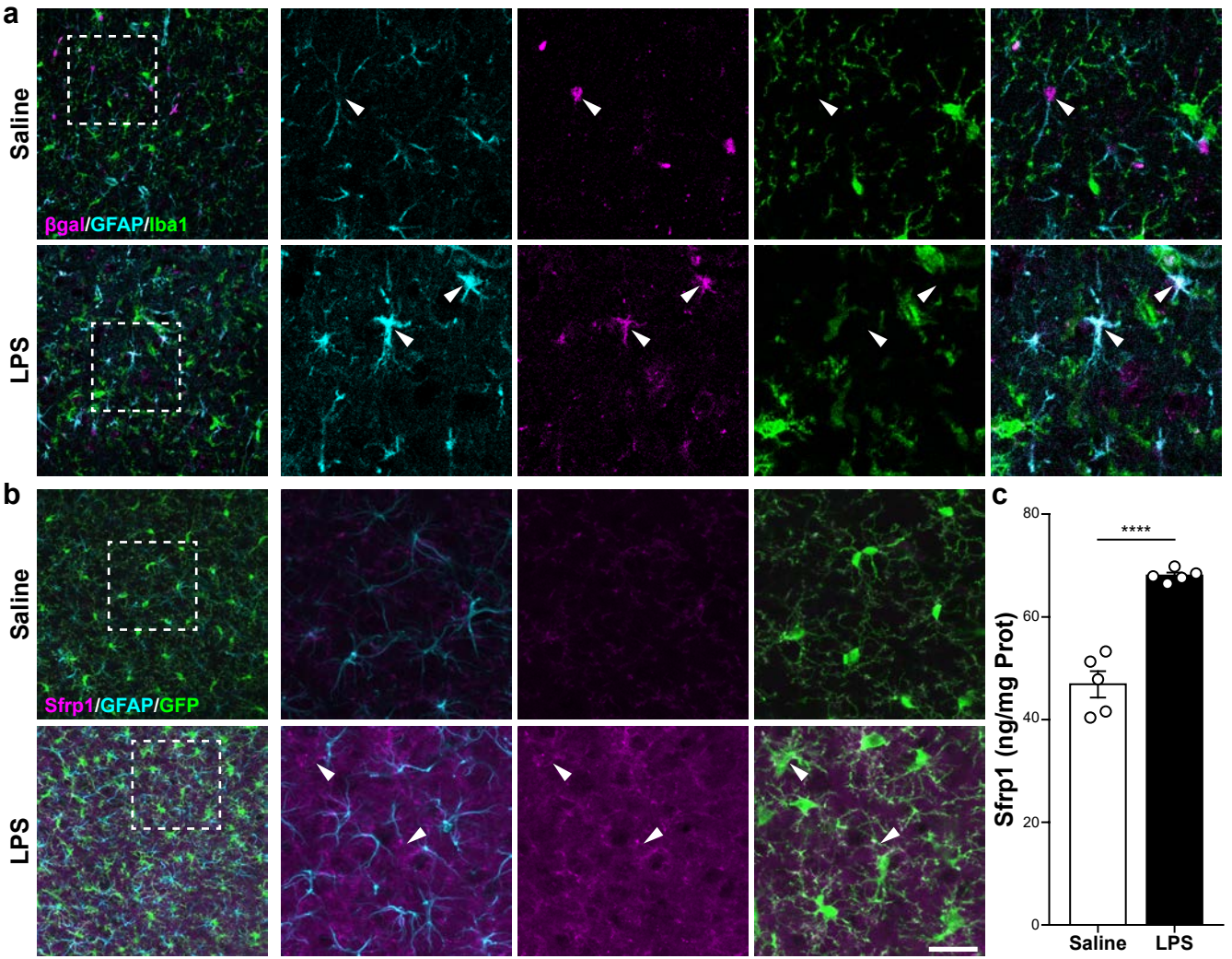
a
Saline
βgal/GFAP/Iba1
LPS
b
Saline
Sfrp1/GFAP/GFP
LPS
c
Sfrp1 (ng/mg Prot)
80
60
40
20
0
****
Saline
LPS

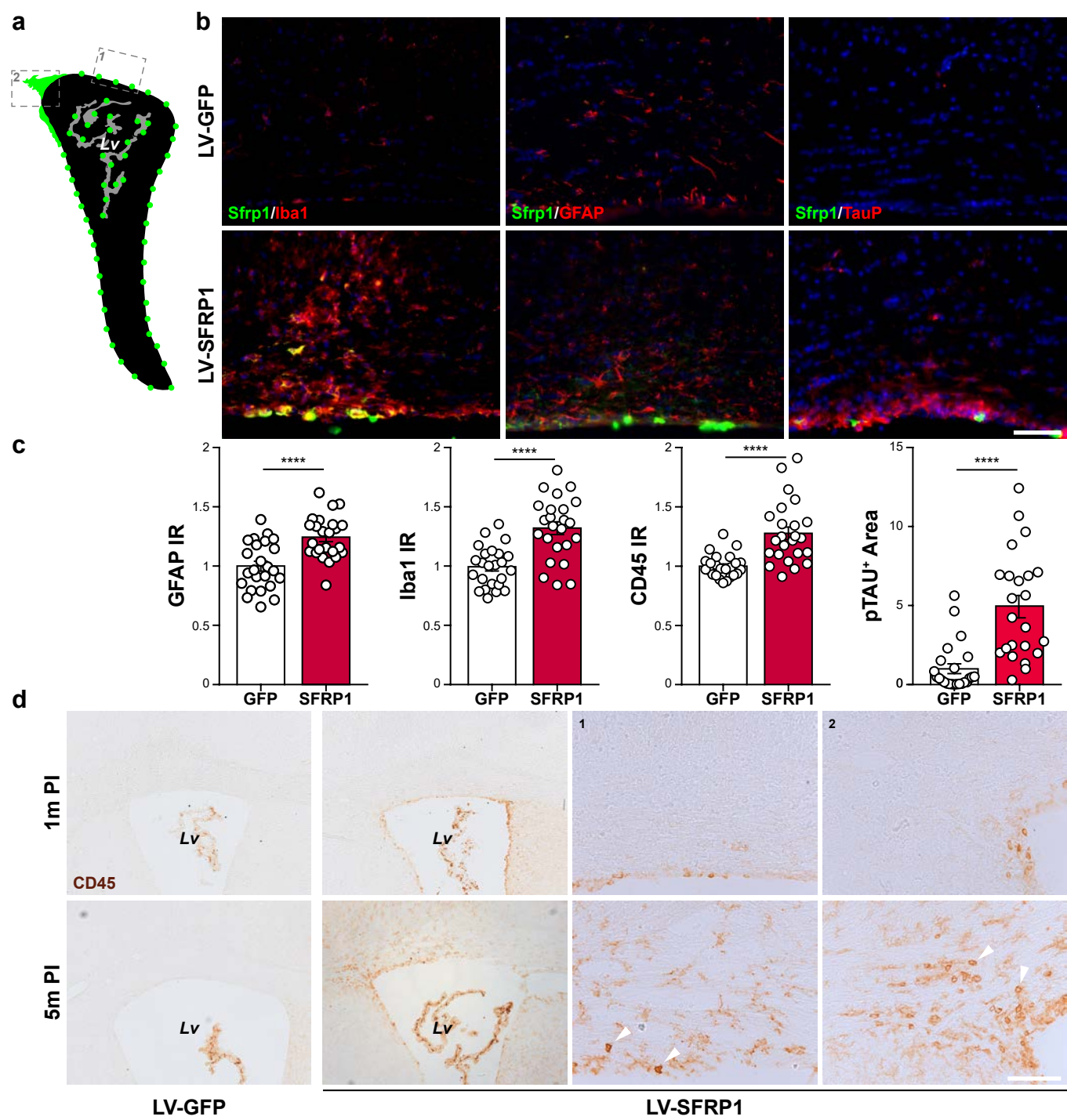
a
1
2
Lv
b
LV-GFP
LV-SFRP1
Sfrp1/Iba1
Sfrp1/GFAP
Sfrp1/TauP
c
GFAP IR
Iba1 IR
CD45 IR
pTAU⁺ Area
****
GFP
SFRP1
d
1m PI
5m PI
CD45
Lv
1
2
LV-GFP
LV-SFRP1

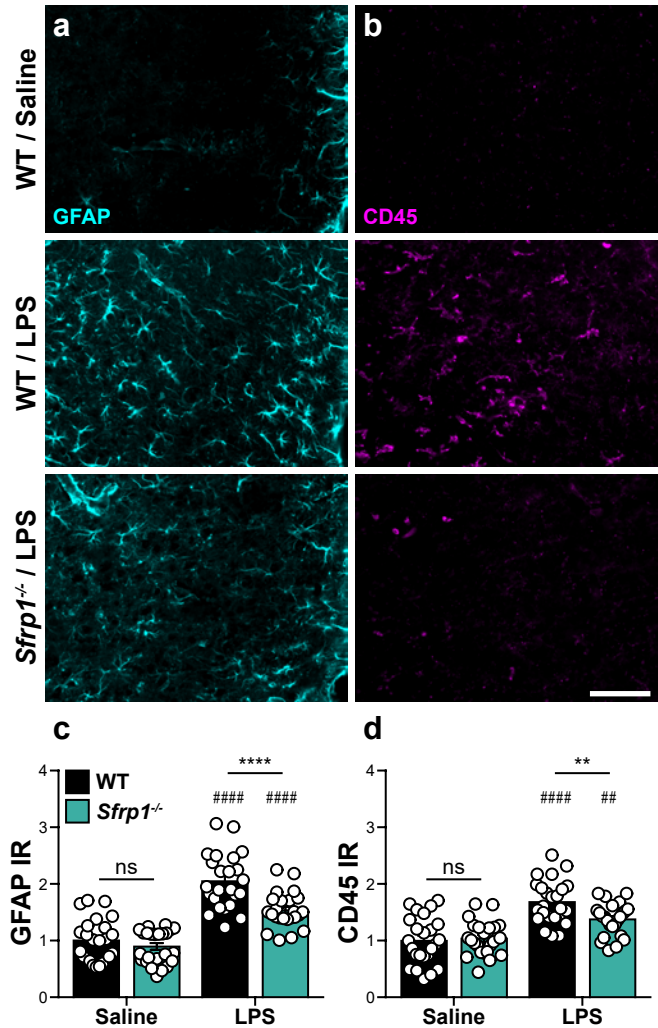
a
b
WT / Saline
GFAP
CD45
WT / LPS
Sfrp1-/- / LPS
c
d
WT
Sfrp1-/-
GFAP IR
CD45 IR
ns
****
**
####
##
Saline
LPS
0
1
2
3
4

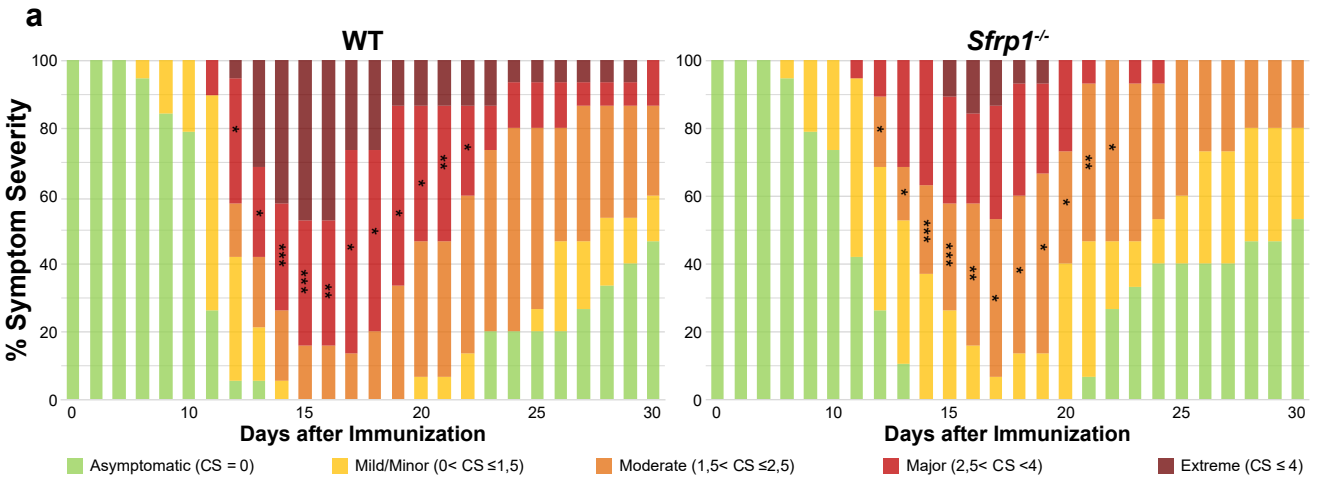
a
WT
Sfrp1-/-
% Symptom Severity
Days after Immunization
Asymptomatic (CS = 0)
Mild/Minor (0< CS ≤1,5)
Moderate (1,5< CS ≤2,5)
Major (2,5< CS <4)
Extreme (CS ≤ 4)

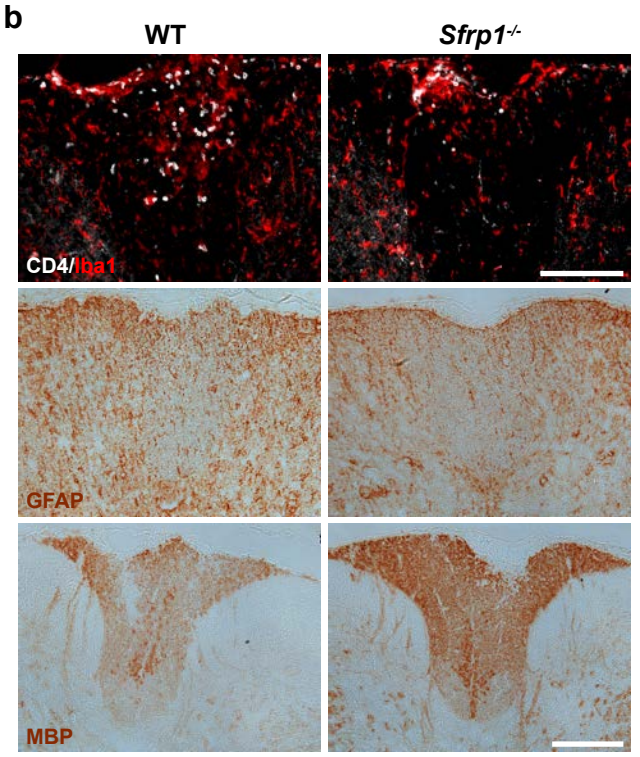
b
WT
Sfrp1-/-
CD4/Iba1
GFAP
MBP

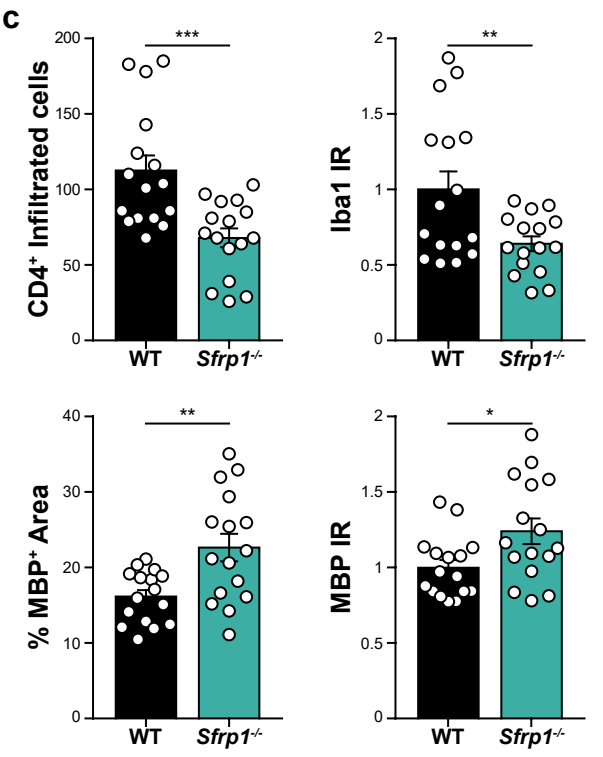
c
CD4+ Infiltrated cells
Iba1 IR
% MBP+ Area
MBP IR
WT
Sfrp1-/-

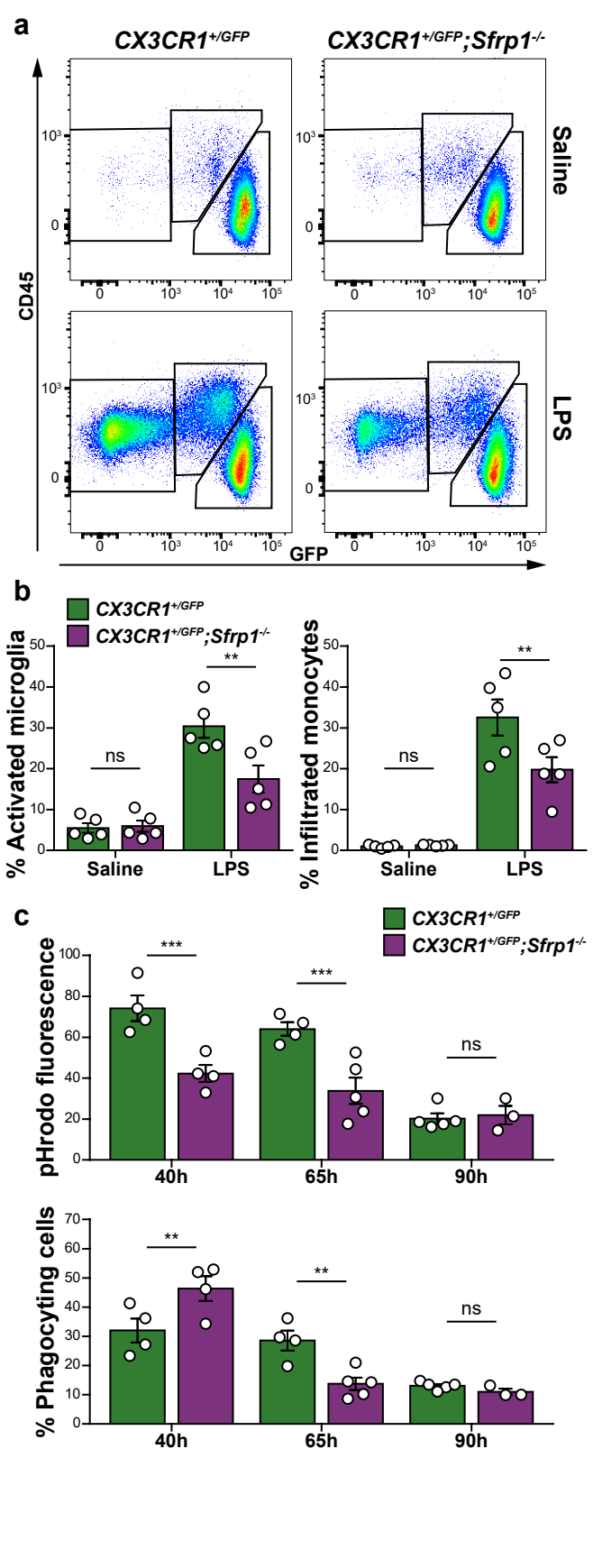
a
CX3CR1+/GFP
CX3CR1+/GFP;Sfrp1-/-
Saline
LPS
CD45
GFP
b
CX3CR1+/GFP
CX3CR1+/GFP;Sfrp1-/-
% Activated microglia
% Infiltrated monocytes
ns
**
Saline
LPS
c
CX3CR1+/GFP
CX3CR1+/GFP;Sfrp1-/-
pHrodo fluorescence
% Phagocyting cells
***
**
ns
40h
65h
90h

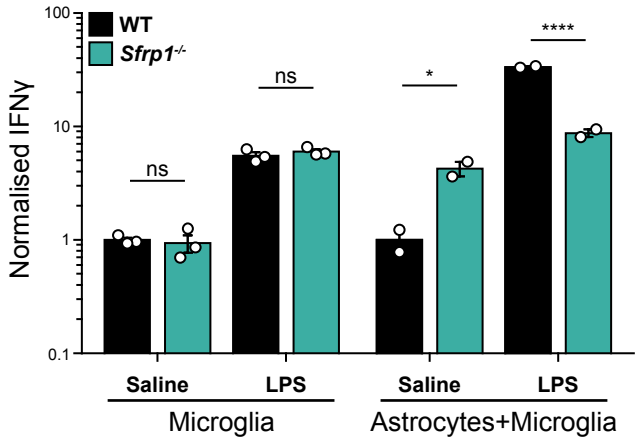
WT
Sfrp1-/-
Normalised IFNγ
100
10
1
0.1
ns
ns
*
****
Saline
LPS
Saline
LPS
Microglia
Astrocytes+Microglia

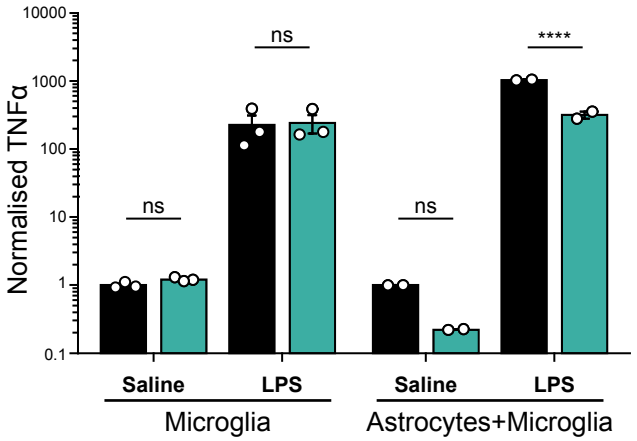
Normalised TNFα
10000
1000
100
10
1
0.1
ns
ns
ns
****
Saline
LPS
Saline
LPS
Microglia
Astrocytes+Microglia

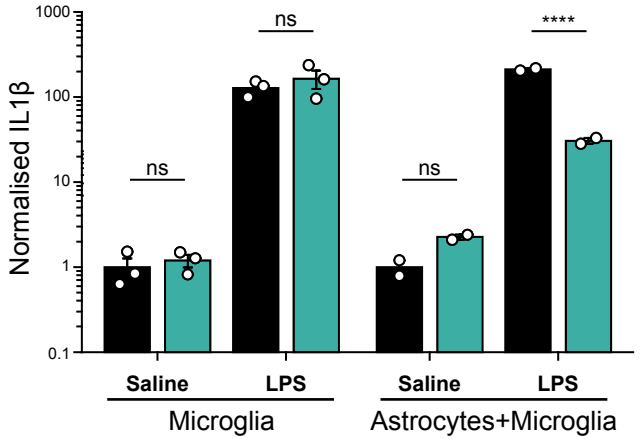
Normalised IL1β
1000
100
10
1
0.1
ns
ns
ns
****
Saline
LPS
Saline
LPS
Microglia
Astrocytes+Microglia

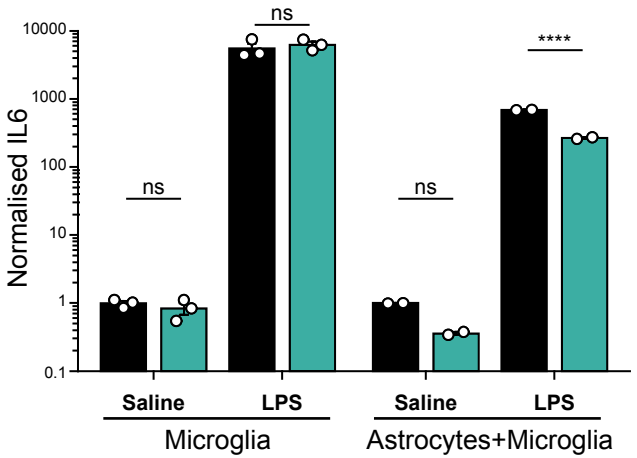
Normalised IL6
10000
1000
100
10
1
0.1
ns
ns
ns
****
Saline
LPS
Saline
LPS
Microglia
Astrocytes+Microglia

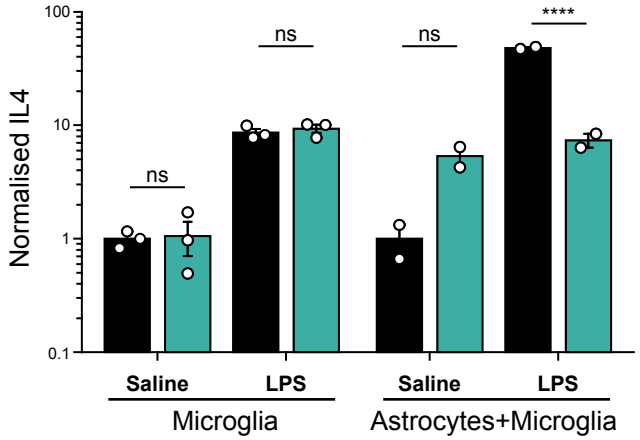
Normalised IL4
100
10
1
0.1
ns
ns
ns
****
Saline
LPS
Saline
LPS
Microglia
Astrocytes+Microglia

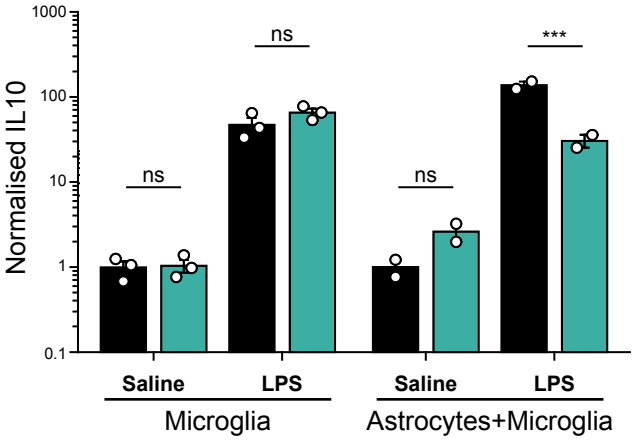
Normalised IL10
1000
100
10
1
0.1
ns
ns
ns
***
Saline
LPS
Saline
LPS
Microglia
Astrocytes+Microglia

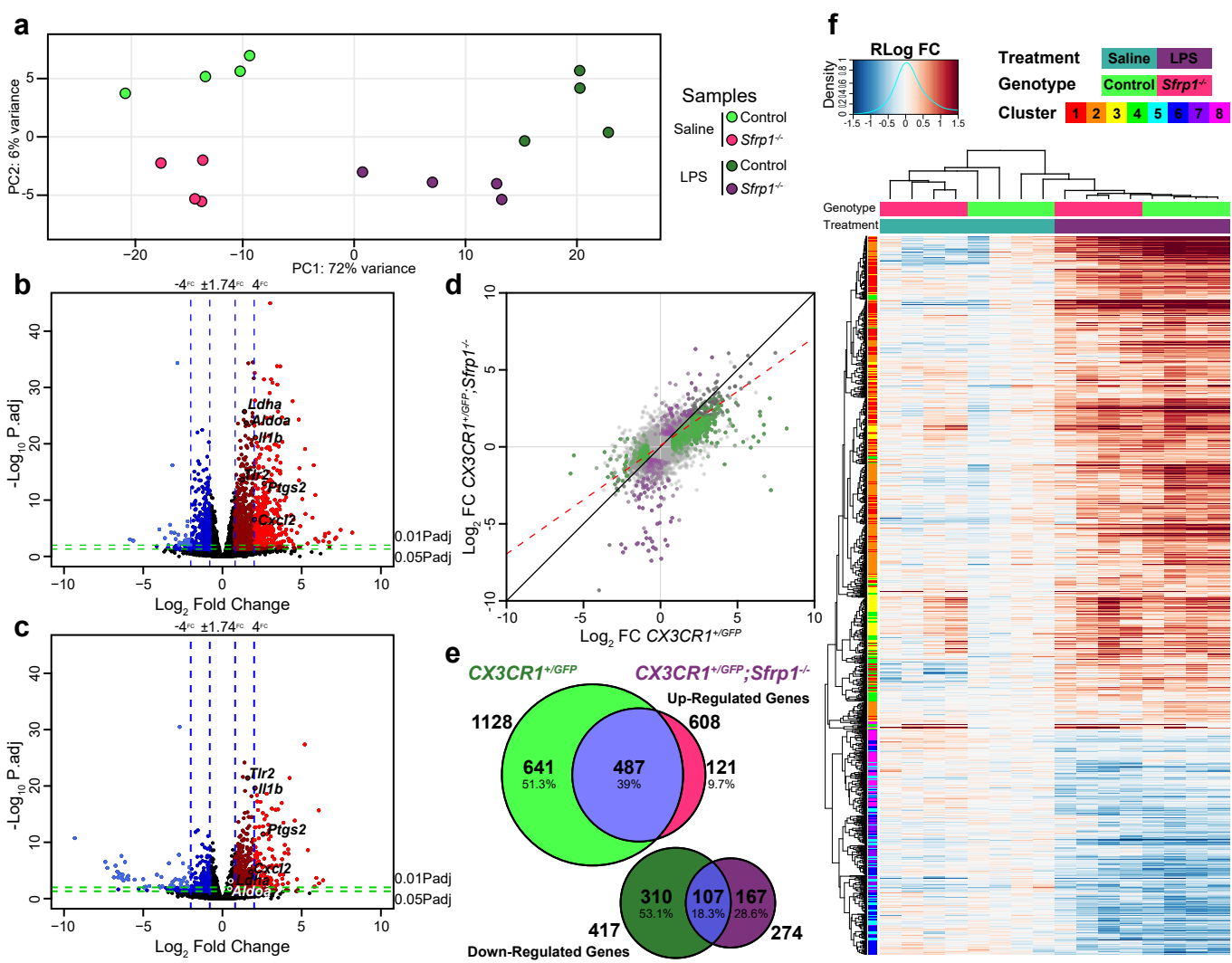
a
PC2: 6% variance
PC1: 72% variance
Samples
Saline
Control
Sfrp1-/-
LPS
Control
Sfrp1-/-
b
-4FC ±1.74FC 4FC
-Log10 P.adj
Log2 Fold Change
Ldha
Aldoa
Il1b
Tlr2
Ptgs2
Cxcl2
0.01Padj
0.05Padj
c
-4FC ±1.74FC 4FC
-Log10 P.adj
Log2 Fold Change
Tlr2
Il1b
Ptgs2
Cxcl2
Ldha
Aldoa
0.01Padj
0.05Padj
d
Log2 FC CX3CR1+/GFP;Sfrp1-/-
Log2 FC CX3CR1+/GFP
e
CX3CR1+/GFP
CX3CR1+/GFP;Sfrp1-/-
Up-Regulated Genes
1128
608
641
51.3%
487
39%
121
9.7%
310
53.1%
107
18.3%
167
28.6%
417
274
Down-Regulated Genes
f
RLog FC
Density
Treatment
Saline
LPS
Genotype
Control
Sfrp1-/-
Cluster
1 2 3 4 5 6 7 8
Genotype
Treatment

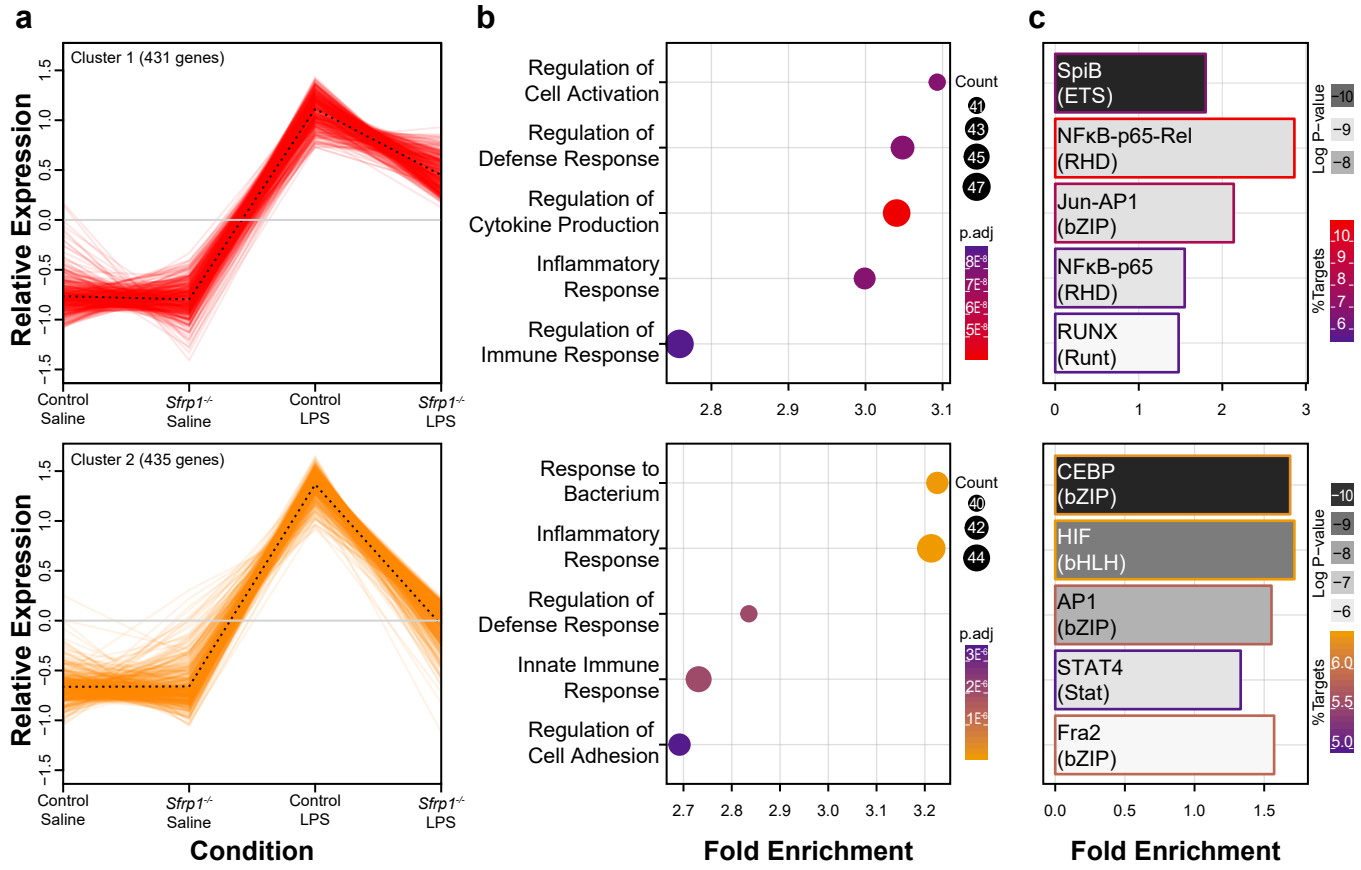
a
Cluster 1 (431 genes)
Relative Expression
Control Saline
Sfrp1-/- Saline
Control LPS
Sfrp1-/- LPS
Cluster 2 (435 genes)
Condition
b
Regulation of Cell Activation
Regulation of Defense Response
Regulation of Cytokine Production
Inflammatory Response
Regulation of Immune Response
Count
p.adj
Response to Bacterium
Inflammatory Response
Regulation of Defense Response
Innate Immune Response
Regulation of Cell Adhesion
Fold Enrichment
c
SpiB (ETS)
NFκB-p65-Rel (RHD)
Jun-AP1 (bZIP)
NFκB-p65 (RHD)
RUNX (Runt)
CEBP (bZIP)
HIF (bHLH)
AP1 (bZIP)
STAT4 (Stat)
Fra2 (bZIP)
Log P-value
% Targets
Fold Enrichment

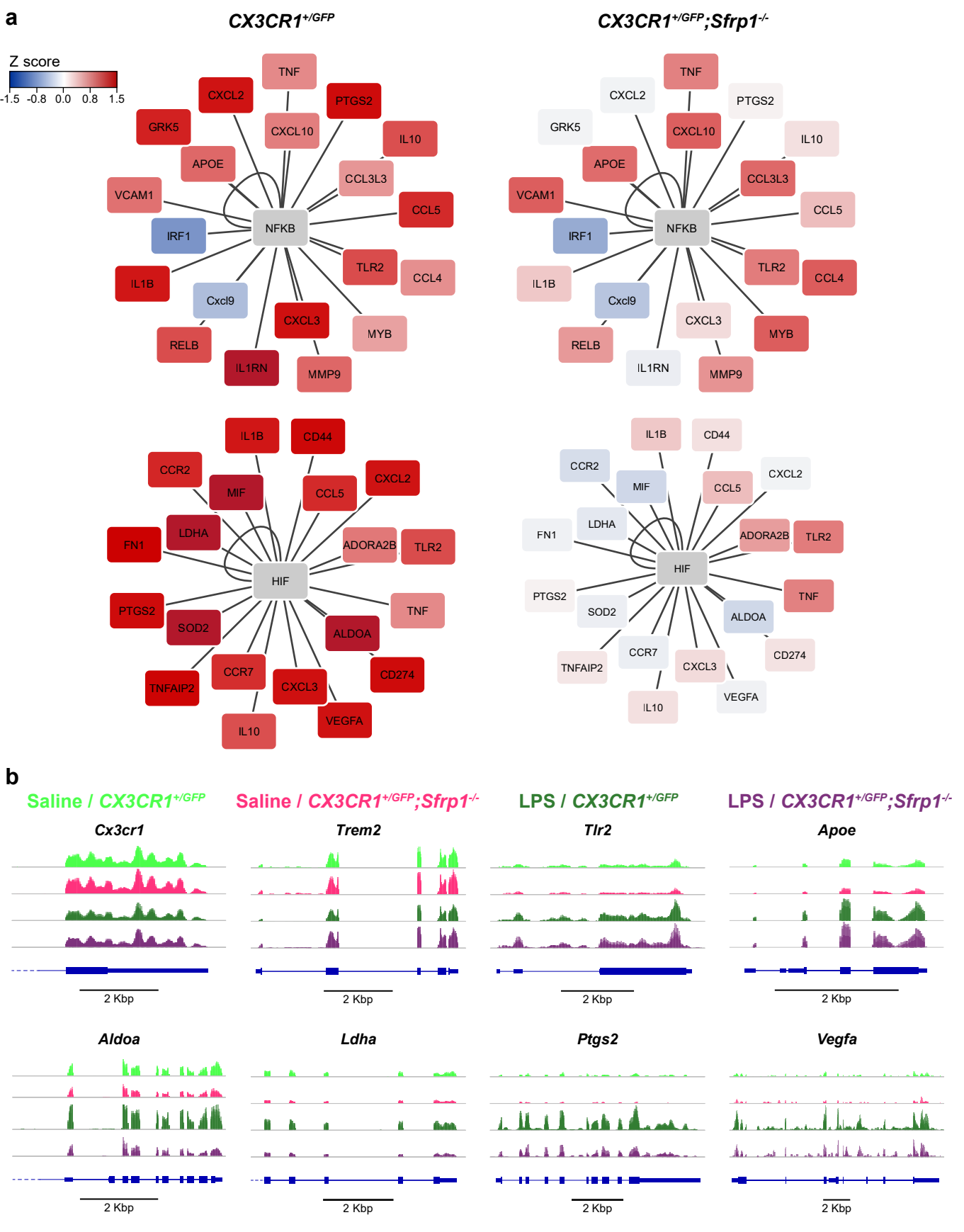
a
CX3CR1+/GFP
CX3CR1+/GFP;Sfrp1-/-
Z score
-1.5 -0.8 0.0 0.8 1.5
NFKB
TNF
CXCL2
PTGS2
GRK5
CXCL10
IL10
APOE
CCL3L3
VCAM1
CCL5
IRF1
TLR2
IL1B
CCL4
Cxcl9
CXCL3
MYB
RELB
IL1RN
MMP9
HIF
IL1B
CD44
CCR2
MIF
CCL5
CXCL2
LDHA
FN1
ADORA2B
TLR2
PTGS2
TNF
SOD2
ALDOA
CCR7
CD274
TNFAIP2
CXCL3
VEGFA
IL10
b
Saline / CX3CR1+/GFP
Saline / CX3CR1+/GFP;Sfrp1-/-
LPS / CX3CR1+/GFP
LPS / CX3CR1+/GFP;Sfrp1-/-
Cx3cr1
Trem2
Tlr2
Apoe
Aldoa
Ldha
Ptgs2
Vegfa
2 Kbp